GEOLOGY FOR SOCIETY

SINCE 1858

GEOLOGICAL
SURVEY OF
NORWAY

· NGU ·

NGU REPORT
2021.035

Hazard and risk assessment of the
Stiksmoen unstable rock slope in
Aurlandfjord (Flåm, Vestland)

NORGES GEOLOGISKE UNDERSØKELSE
- NGU -

REPORT

Geological Survey of Norway
P.O.Box 6315 Torgarden
NO-7491 TRONDHEIM
Tel.: 47 73 90 40 00

Title:
Hazard and risk assessment of the Stiksmoen unstable rock slope in Aurlandfjord (Flåm, Vestland)

Authors: Penna, I.M., Nicolet, P., Bredal, M., Böhme, M., Kristensen, L., Pless, G., and Eiken, T.

Client:
Norges vassdrags og energidirektorat (NVE)

County: Vestland

Municipality: Flåm

Map-sheet name (M=1:250.000)

Map-sheet no. and -name (M=1:50.000)

Deposit name and grid-reference:

Number of pages: 44
Map enclosures:

Price (NOK): 160

Fieldwork carried out:
08/2014-04/2021

Date of report:
13.01.2022

Project no.:
310100

Person responsible:

Summary:

Stiksmoen is located on a west-facing slope at approximately 120 m a.s.l. in the southern end of Aurlandfjord (Flåm municipality, Vestland county). The unstable rock slope is bounded by a well-developed backscarp, wide open in the north and open but less developed in the southern sector. The lower limit is mapped close to the foot of the frontal cliff of the unstable rock mass. The upper and central part of the instability is characterized by the presence of several open cracks, 10 to 15 meters deep. High rockfall activity is observed in the frontal cliff, with the detached blocks forming a block field. Structural and geophysical surveys allowed for the reconstruction of the sliding surface of Stiksmoen and the computation of its volume (ca. 0.4 million m³). Extensometers, dGNSS, ground-based and satellite-based radar measurements show similar displacement rates in the upper-central part and on the lower-frontal part of the unstable rock mass. The obtained displacement rates range from 0.9-2.5 cm/y towards the west, with a dip of ca. 30°. The degree of development of the Stiksmoen unstable rock slope, its structural characteristics and displacement rate result in a high hazard level. A sudden collapse of the whole unstable rock mass would result in rocks propagating mostly towards the fjord and a small proportion in WSW direction (towards Viki). The direct impact of the rock mass into the fjord would cause a displacement wave that could result in the loss of lives. The high hazard level and the potential consequences in the direct and secondary impact area result in a high-risk level for Stiksmoen.

| Keywords:	Unstable rock slope	Flåm
Hazard	Risk	Stiksmoen
Stampa		

Contents

1. Introduction

The Norwegian Geological Survey (NGU) carries out a systematic mapping of unstable rock slopes in Norway. The hazard and risk assessment are part of the national plan for mapping unstable rock slopes and has since 2009 been financed by the Norwegian Water Resources and Energy Directorate (Devoli et al., 2011, Øydvin et al., 2011; Blikra et al., 2016). A systematic survey of aerial photos, digital elevation models and InSAR data has allowed for the identification of more than 630 unstable rock slopes up to the present date. Their volumes range from a hundred thousand cubic meters up to several millions of cubic meters. The hazard assessment carried out includes the detailed characterization of the unstable rock slopes, and the assessment of their potential direct impact area and secondary hazards (displacement waves in fjords and lakes, and the formation of natural dams (e.g. Devoli et al., 2011, Hermanns et al., 2012; Oppikofer et al., 2016a; Oppikofer et al., 2021)).

To date, one of the largest unstable rock slopes identified in Norway is Stampa, which is located in the eastern slope of the Aurlandfjord (Domaas et al., 2002; Braathen et al., 2004; Hermanns et al., 2011a and b; Blikra et al., 2013; Böhme et al., 2013; Kristensen and Anda, 2016; among others). Stiksmoen, at around 120 m a.s.l. in the southern end of the Aurlandfjord, in front of Flåm harbour, locates on the same slope as Stampa (Figure 1 and Figure 2).
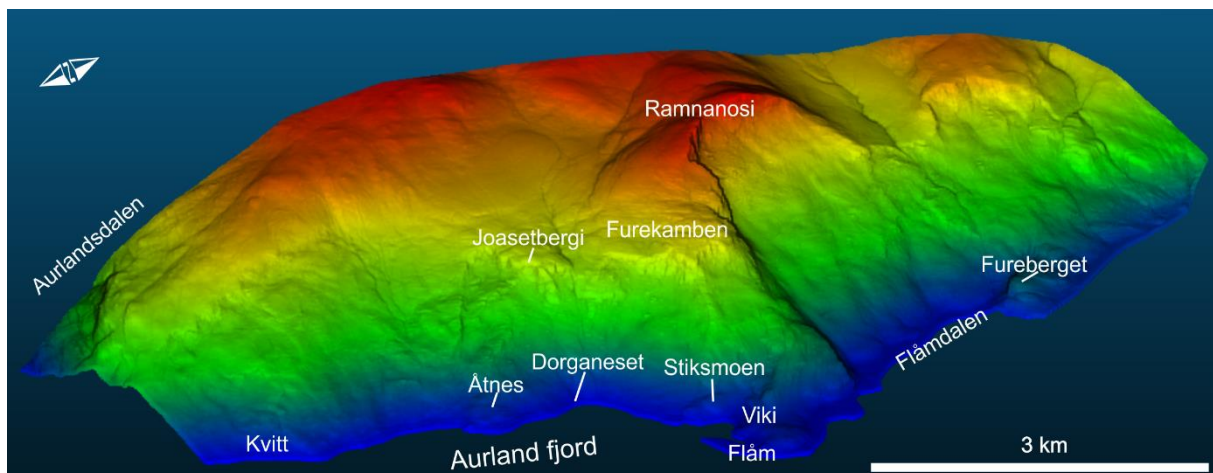
Figure 1. 3D view of the Stampa unstable rock slope with indication of the localities mentioned in the text.
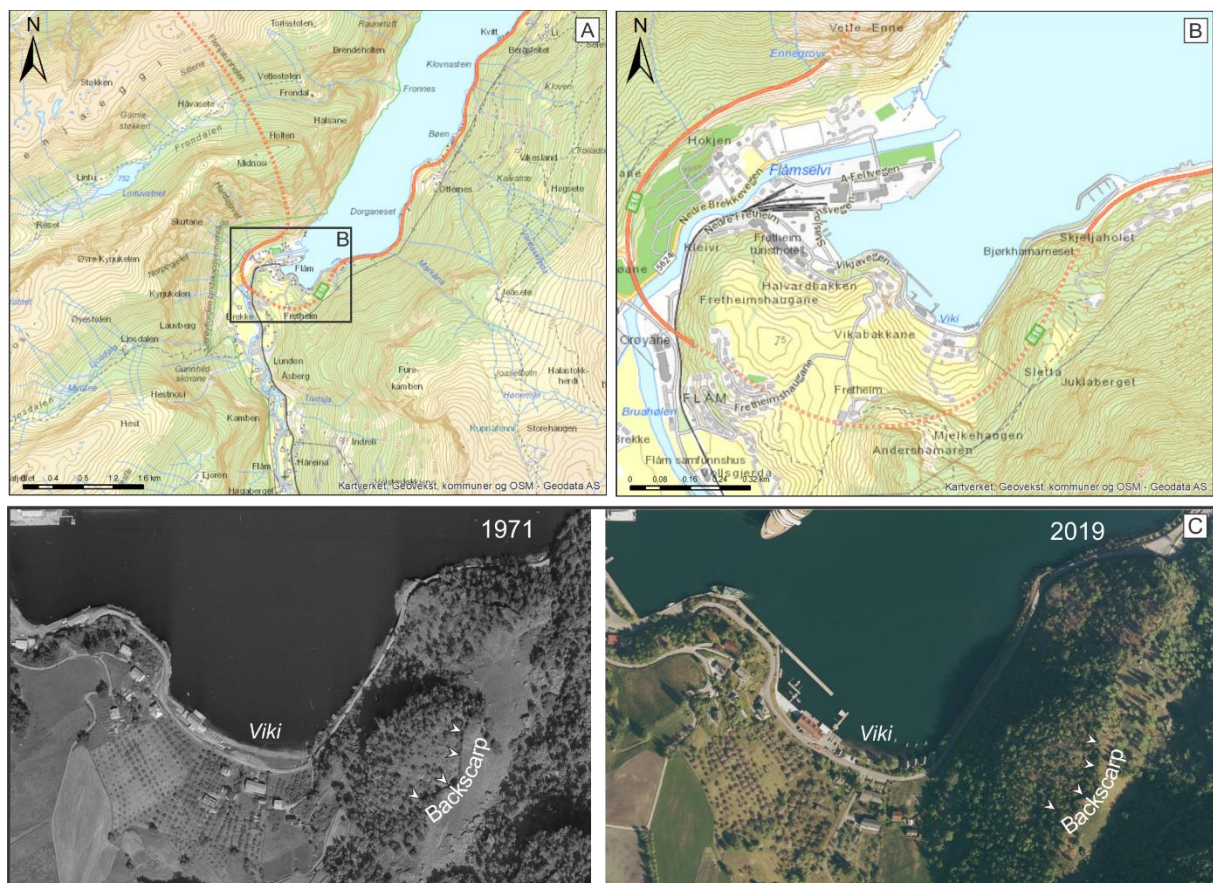
Figure 2. A) View to the southern end of the Aurlandfjord. B) Detailed view of Flåm and the location of the unstable rock slope. C) Aerial photos showing the unstable rock slope in 1971 and 2019.

Stiksmoen was studied in the late 1970s during the construction of the Fretheim tunnel pointing out activity on this part of the slope (Grimstad, 1978). Grimstad (1987) measured displacements of 4-5 mm/y, between 1978 and 1987, on the open cracks developed in the upper part of Stiksmoen. In 2015, NGU mapped the area and installed two extensometers and one global satellite-based navigation system (dGNSS) point on the unstable rock slope and one fix point on assumed stable rocks. These dGNSS points expand extensive network of dGNSS points installed in Stampa. Since 2015, geological fieldwork has been conducted at the site every field season. Interferometric synthetic aperture radar (InSAR) data, from Sentinel 1 satellites, extends over several years. Although the area is vegetated, the upper central part can be detected by the satellites, and the displacement rates obtained are consistent with other observations. In 2018 and 2019, NVE scanned the sites with a Ground-based InSAR.

In the following sections, we present the results of the surveys carried out so far in Stiksmoen, which have allowed for the site hazard and risk classification.

2. General setting

Detailed geological background information of Stampa can be found in Braathen et al. (2004), Hermanns et al. (2011a), Böhme et al. (2013), Blikra et al. (2013) and NGU (2020). We summarize the main geologic and geomorphologic features below and describe the unstable rock slope. The location of the main localities referenced in the text can be seen in Figure 1.

2.1 Geology and landscape conditions

The phyllites, were the unstable rock slope developed (Figure 3), were strongly deformed during the Caledonian orogeny and thrusted over Precambrian basement. The phyllites are highly deformed with folds ranging from centimeters to meters (Böhme et al., 2013). In Stampa, major fractures present NE-SW and WNW-ESE orientation and high angles (ca. 80°), and foliation dips range between 16° to 35° towards the SW.

Past glaciations have left a strong imprint on the landscape of the area. U-shaped valleys lead to fjords with steep walls. Debuttressing and isostatic rebound, because of glacial retreat, have been proposed as contributing factors for slope instabilities in western Norway (Blikra et al., 2006). The marine limit in Aurlandfjord lies at 130 m a.s.l. Above Stiksmoen, there is a flat area called Sletta (Figure 3) which presents a marine sediment coverage of ca. 25 m thick, according to GPR data (Tassis and Larsen, 2021).

From Aurland to Flåm, the eastern slope of the Aurlandfjord presents a thick cover of scree deposits. Geophysical data and topographic reconstructions indicate that in some sectors of the slope the thickness of these deposits reaches 50 m (Blikra et al., 2013).
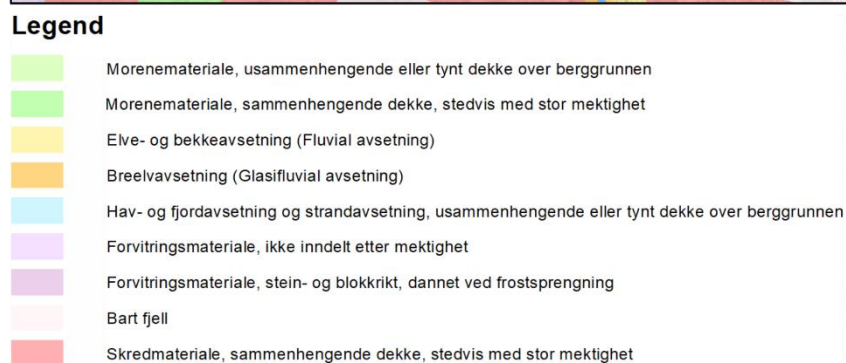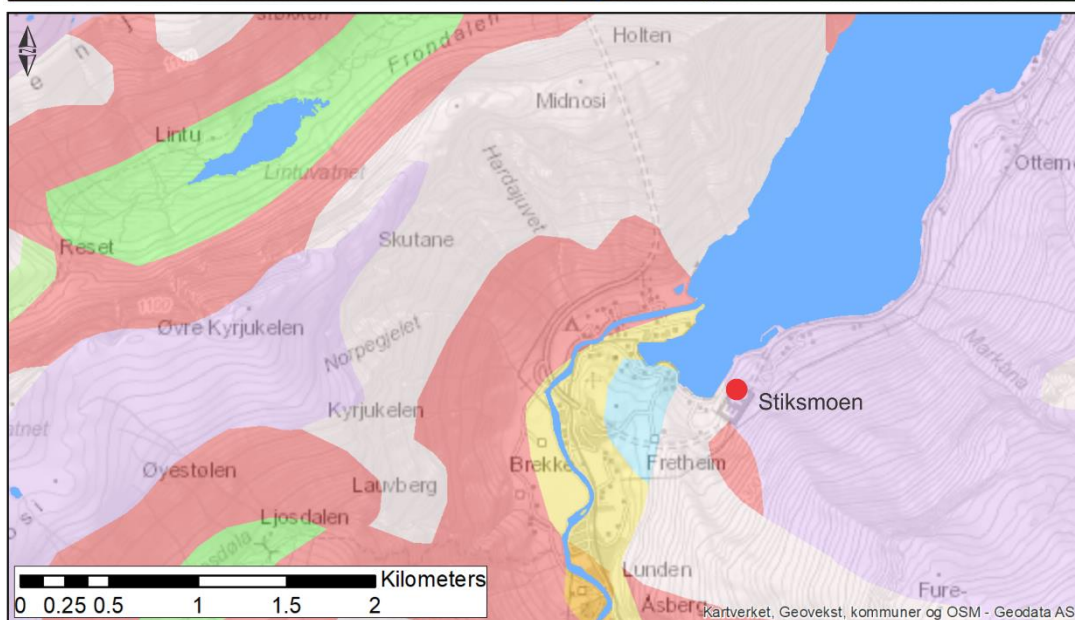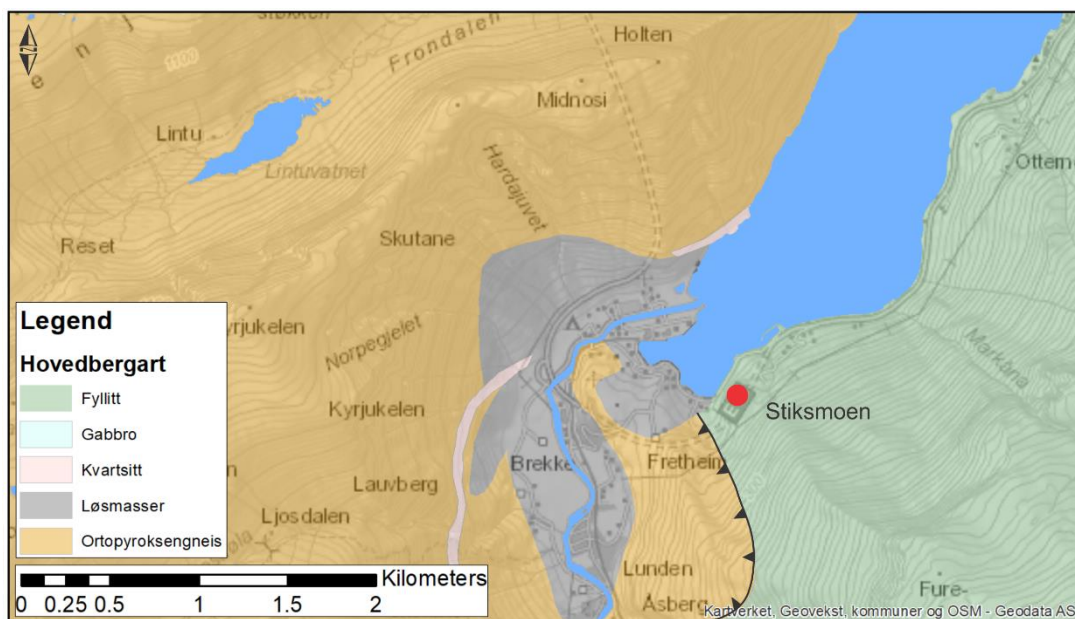
*Figure 3. A) Geologic map of Flåm area (modified from NGU 1:50000 series; Bryhni, 1977)
over topographic. B) Quaternary map of Flåm area (modified from NGU 1:250000 series).*

2.2 Slope deformation and past slope collapses

From Ramnanosi (Flåmdalen) to Kvitt (south of Aurland), the eastern flank of the valley shows signs of gravitational deformation (Braathen et al., 2004; Blikra et al., 2006; Hermanns et al., 2011a; Böhme et al., 2013). The gravitational deformation affects the outcropping rocks and, in some places, such as in Dorganeset or right downslope Ramnanosi (see locations in Figure 1), the block fields that cover the slope are actively displacing downslope. In Dogarneset, the displacement rate of the block field is ca. 2 cm/y according to InSAR data (see insar.ngu.no). The morphology of the moving block field and some other features observed in bathymetric information suggest that the deformation continues below the sea level. A burst event (sudden increase in the displacement) occurred in the summer of 1979; Domaas et al. (2002) documented a rapid displacement of these deposits, which resulted in material falling into the fjord.

On the upper part of Stampa, the largest open cracks developed along fractures generated during the Caledonian orogeny. In Ramnanosi, these cracks are mainly oriented NNW-SSE, while from Furekamben to Kvitt the opening takes place mainly along NE-SW structures (Blikra et al., 2013).

Past failures detached from the southeastern slope of Aurlandfjord deposited significant amounts of debris at water depths of 80-100 m (Blikra et al., 2006). On the fjord bottom, past failures are observed as lobate landforms with large-scale boulders on the surface (Blikra et al., 2002; Blikra et al. 2006). Blikra et al. (2002), points out the possibility of a two-stage formation of failures which involves the phyllites in Aurland area: one event occurred shortly after the deglaciation and another smaller event occurred at ca. 3000 cal. BP.

3. Methods

3.1 Structures and kinematic analyses

The phyllites in Stiksmoen are affected by different types of discontinuities (different sets of foliation and fractures). During field work, the orientation of these structures was measured at 20 sites using a compass, and each structure's dip and dip direction was measured (Figure 4). The spatial arrangement of discontinuities conditions the stability of the rock mass and the kinematics of its deformation. In this work, the orientation data was used to perform kinematic analyses of slope stability using the software Dips, version 7.0 (Rocscience.com).
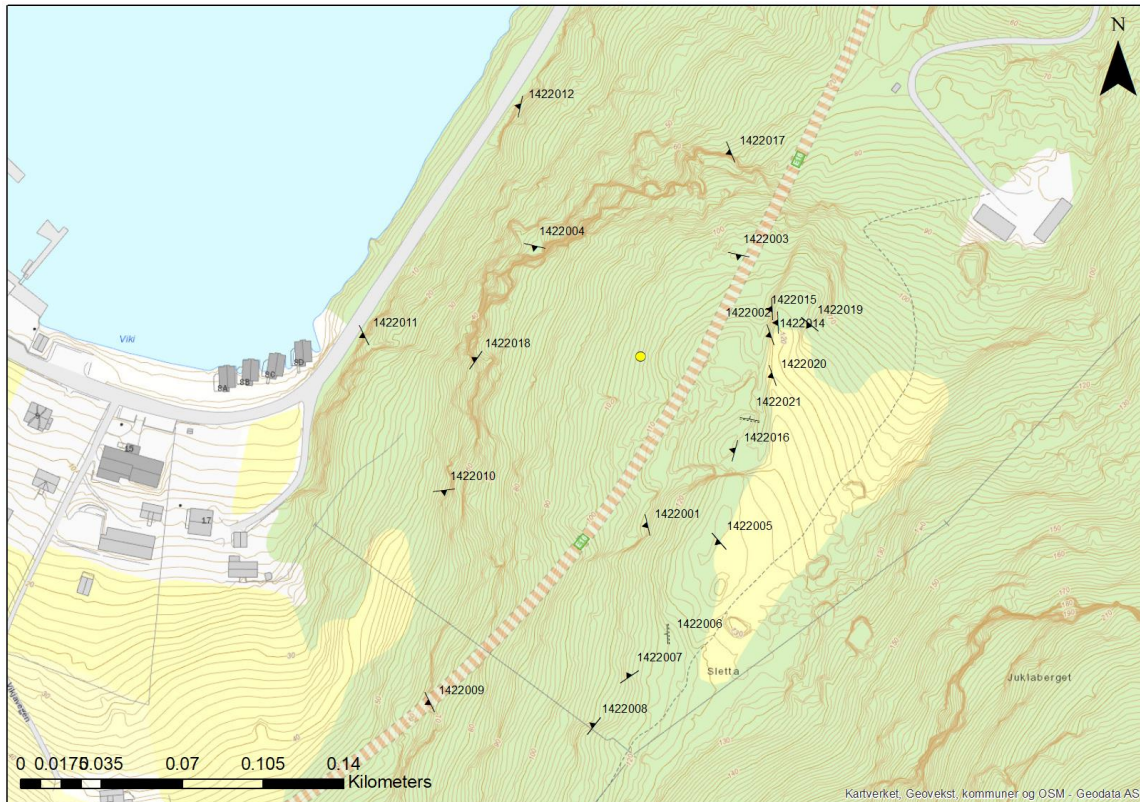
Figure 4. Location of sites where structural measurements were performed.

3.2 Displacement measurements

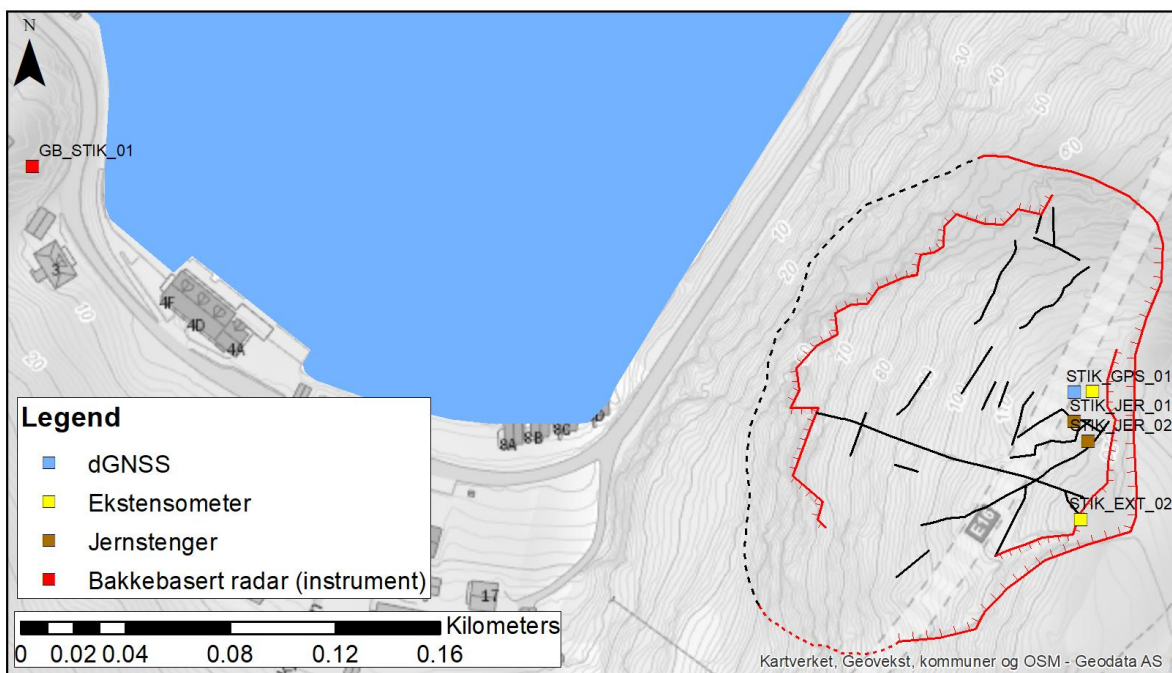The displacement rate of Stiksmoen has been determined using *in situ* and remote measurement techniques (Figure 5).

Figure 5. Map showing the limits of the unstable rock mass and the location of the dGNSS, extensometers and GB-InSAR stations.

9

Differential Global Navigation Satellite Systems (dGNSS): In Stiksmoen, one rover point was installed (Figure 5). The point became part of the network with 32 stations that have been installed at Stampa between Ramnanosi and Otternes. This dGNSS network has reference points both in the valley bottom and in the plateau area. The measurement of the dGNSS point on Stiksmoen took place at least once a year since 2016. During the measurement, a dGNSS antenna was mounted on the bolts fixed to the outcrops for each acquisition campaign. Static phase measurements were performed with an interval of ca. one year between acquisitions. The measurements were then post-processed using the reference points set in the upper and lower part of Stampa. The displacement rate was considered significant when it meets the following two conditions:

- the displacement rate obtained by linear regression (v) is higher than the average measurement accuracy (σ_{tot}) multiplied by the square root of two and divided by the time interval between the first and the last measurement (Δt) in years:

$$v > \frac{\sqrt{2} \cdot \sigma_{tot}}{\Delta t}$$

- the displacement follows a coherent trend over the years.

Tape extensometers: Two locations to measure displacements were chosen in the backscarp of the instability (Figure 5). The bolts were mounted on both sides of the backscarp. The year of installation was 2016, and since then, measurements have been taken with an interval of ca. one year. The change in the length of the tape extensometer over time corresponds to the displacement rate.

Satellite Interferometric Synthetic Aperture Radar (InSAR): This technique compares microwave images acquired at different times by satellites, allowing for the detection of surface displacements of the order of few millimeters by analysing changes in the phase of the returned microwave (Massonnet and Feigl, 1998). The accuracy of this method depends on the angle formed by the line of sight of the radar and the vector of displacement of the unstable rock slope. The data used in our study was acquired by the Sentinel-1 radar satellites, between 2015 and 2019 (freely available at insar.ngu.no).

Ground-Based InSAR: This technique is based on the same principles as the satellite InSAR. In Stiksmoen, NVE conducted measurements with a LiSALab ground-based radar system (NVE internal report). In order to detect as much as possible of the full displacement of the instability (resulting from the relationship line of sight-vector of displacements), the instrument was mounted on the ground on a property located above Vikjavegen, in the Viki area (Figure 5).

Therefore, the line of sight was roughly parallel to the expected displacement vector. The measurements were performed as campaigns as indicated in Table 1, and the displacement was determined as change in distance between the individual campaigns.

Table 1. Periods of measurements in GB-InSAR in Stiksmoen

	Stiksmoen (Periodic)
1st. measurement	07. june – 14. june 2018
2nd. measurement	06. september – 11. september 2018
3rd. measurement	13. may – 20. may 2019
4th. measurement	03. july – 19. july 2019

3.3 Geophysical surveys

In April 2021, a geophysical survey was carried out in Stiksmoen. The survey consisted of 5 Electrical Resistivity Tomography profiles (ERT; Figure 6) and 2 Ground Penetrating Radar (GPR) lines. The ERT method was chosen because it allows for mapping the contrasts in bedrock that result from different degrees of rock fracturing, water content, mineralization, etc. The ERT profiles were done using a Multiple Gradient array and 5 meters of electrode spacing. Four ERT profiles are SE-NW oriented, which means that they cross the unstable rock slope in the sense of the vector of displacement. One ERT profile was oriented NE-SW and crosses the unstable rock slope perpendicular to the other profiles in its upper-central part. A detailed description of the survey and processing of data can be seen in Tassis and Larsen (2021).
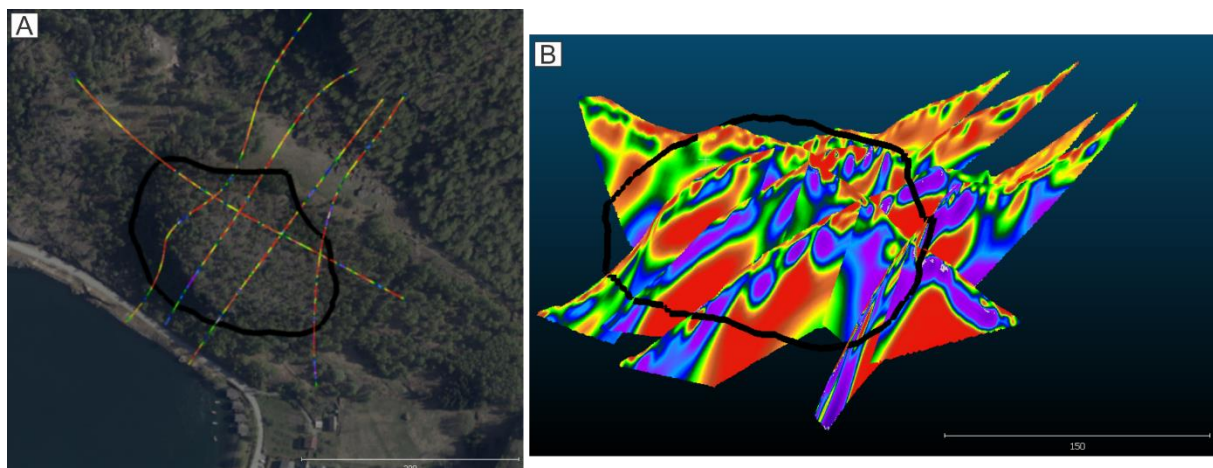
Figure 6. Location of the ERT profiles and the limit of the unstable rock slope B) 3D View of the ERT profiles and the limit of the unstable rock slope (black line).

3.4 Volume calculation

The volume of the unstable rock mass was determined by reconstructing its sliding surface in Cloud Compare and later computed in ArcMap. In Cloud Compare we mapped the sliding surface along the 4 ERT lines crossing the unstable rock mass in E-W direction. Along each ERT line, the sliding surface was mapped assuming that it follows the very low resistivity clusters or areas where conductive layers (graphite) are found on top of resistive ones. The horizons mapped along the ERT lines and the line representing the limit of the sliding surface were converted into points; then, a *Poisson surface* tool was applied in Cloud Compare. After this first reconstruction, manual adjustments were made to correct some errors in the interpolation, and according to observations and structural measurements done during fieldwork. As a final step we used the *Raster Calculator* tool in ArcMap to create a raster representing the thickness of the unstable rock mass. This was done by subtracting the 2014 Songdal_Aurland_Lærdal 50 cm resolution DEM to the sliding surface. The volume of the unstable rock slope resulted from the sum of the thickness values multiplied by the area of a single cell.

3.5 Run-out analyses with DAN3D

The potential area of propagation of the rock mass was modeled using the DAN3D software (McDougall and Hungr, 2004). The software requires as input data: 1) the thickness of the sliding mass (source), and the path topography (aerial and underwater), 2) the control parameters, and 3) the rheological parameters (McDougall and Hungr, 2004; Hungr and McDougall, 2009). The thickness of the sliding mass results from reconstructing the potential basal failure surface, as mentioned in chapter 3.4, and the path topography is the relief along which the rock mass displaces and is the result from the subtraction of the current DEM and the thickness of the unstable rock mass.

The control parameters refer to: 1) the number of particles (higher amount, higher resolution of the model), 2) the smoothing coefficient of particles (relates to the smoothness of the interpolated flow depth), and 3) the velocity smoothing coefficient (the influence of the neighboring particles on the central particle). For our models, we used 2000 particles and no smoothing coefficients.

The combination of the Frictional and Voellmy rheology was used to model the propagation of the rock mass. The first was used for the subaerial part and the second for the submerged part. The combination of these two rheologies was used in previous studies for landslides propagating into water bodies (e.g. Mazzanti et al., 2010; Mazzanti and Bozzano, 2011; Penna et al., 2017).

Because of the lack of accurate back-analysis of past rockslide dynamics in the area, we defined 10 model setups with changing conditions on the subaerial part and fixed parameters on the submerged part (Table 2). The wide range selected aimed to obtain the area where the rock mass would propagate and deposit. The limits of the range of parameters were set by considering back-analyses done in other mountain settings (e.g. Hungr and Evans, 1996; Sosio et al., 2008), and the modelled run out was compared with the volume/travel of reach relationship for landslides (Scheidegger 1973).

Because of the closeness to the water, the run-out of the rock mass in the subaerial part will be around 40-50 m long. The scree material accumulated at the toe of the unstable rock mass could be entrained during a sudden collapse, but since the volume is considered very minor with regards to the total volume of the unstable rock mass, entrainment was not addressed in the models. We lack information about the type and thickness of sediments on the submerged part of the slope, as well as the extent of the effects that a rock mass could have on the loose materials present in the fjord. Potential secondary effects such as the collapse of sediments or landfills close to the shoreline or the deformation of loose materials on the fjords floor, caused by the displacement wave or the rock mass propagating in the fjord, are not addressed in this study.

Table 2. Parameters selected for the dynamic models of Stiksmoen.

Model	Part	Rehology	Unit weight	FA	FC	t	IFA	Pu
T1	Subaerial	Frictional	27	29				29	0.1
	Submerged	Voellmy	25		0.2	250	32	
T2	Subaerial	Frictional	27	24				29	0.1
	Submerged	Voellmy	25		0.2	250	32	
T3	Subaerial	Frictional	27	32				29	0.1
	Submerged	Voellmy	25		0.2	250	32	
T4	Subaerial	Frictional	27	21				29	0.1
	Submerged	Voellmy	25		0.2	250	32	
T5	Subaerial	Frictional	27	29				25	0.1
	Submerged	Voellmy	25		0.2	250	25	
T6	Subaerial	Frictional	27	24				25	0.1
	Submerged	Voellmy	25		0.2	250	25	
T7	Subaerial	Frictional	27	32				25	0.1
	Submerged	Voellmy	25		0.2	250	25	
T8	Subaerial	Frictional	27	21				25	0.1
	Submerged	Voellmy	25		0.2	250	25	
T9	Subaerial	Frictional	27	29				27	0.1
	Submerged	Voellmy	25		0.2	250	25	
T10	Subaerial	Frictional	27	24				27	0.1
	Submerged	Voellmy	25		0.2	250	25	

FA= Friction Angle (degrees); FC= Friction coefficient (dimensionless); t= Turbulence (m/s_2); IFA= Internal friction angle (degrees). Pu: pore pressure coefficient (dimensionless)

By combining the maximum propagation of each model, we obtained a propagation probability map representing the area that could potentially be affected by the direct propagation of the rock mass.

3.6 Hazard and risk assessment

3.6.1 Hazard classification
The methodology used for the hazard classification of Stiksmoen can be seen in Hermanns et al. (2012).

3.6.2 Consequence assessment
In this report, the consequences are only addressed as potential losses of life in the direct impact area resulting from the modelling of the propagation of the rock mass and in the displacement wave area modelled by Glimsdal (2022). Detailed information about the methodology for the consequence assessments can be seen in Oppikofer et al. (2016b).

In the direct impact area: The consequences in this area were computed considering the amount and type of buildings in the subaerial part of the propagation path of the rock mass.

In the displacement wave area: Here the consequences are computed considering the amount and type of buildings in the run-up zone of the displacement wave. In addition, the consequence assessment considered the number of tourists visiting the area, which can be especially significant between April and October. There are no statistics about the number of tourists visiting Flåm every year. In this study, we have computed the consequences considering 1 million per year, which is mentioned as an estimation in Nicolaisen (2020). Between 2012 and 2019, ca. 150 cruise ships per year arrived to Flåm (Nicolaisen, 2020). In 2022, 114 cruises are estimated to arrive to Flåm (source: https://www.flamport.no/ship-arrivals2021.

Exposure is assumed to be 100% for permanent residents, 75% for tourists and varies according to Oppikofer et al. (2016b) for persons in buildings where there are no permanent residents. Vulnerability is assumed to be 100% in the direct impact area, and 70% in the tsunami area.

3.6.3 Risk Classification
Risk classification is obtained through the matrix presented in Hermanns et al. (2012). However, since the hazard zones for the displacement wave are given for predefined probabilities, namely 1/1000 and 1/5000, and not for the probability of rupture, consequences can't be plotted in the matrix directly against the probability of rupture. Therefore, the consequences are calculated for each scenario and multiplied by the corresponding probability

to obtain the total risk. This allows eventually to calculate the corresponding consequences that can be plotted in the matrix. To calculate the risk of the area inside each hazard zone, an average probability is considered as follow:

$$\begin{cases} p_{1000} = 0.5 \cdot \left(\dfrac{1}{p_{direct}} + \dfrac{1}{1000} \right) \\ p_{5000} = 0.5 \cdot \left(\dfrac{1}{1000} + \dfrac{1}{5000} \right) \end{cases}$$

Indeed, using directly the probability corresponding to the hazard zone would result in an underestimation of the risk (see Nicolet, 2017). Then, the partial risk for each scenario can be calculated as follow:

$$\begin{cases} R_{direct} = (p_{direct} - p_{1000}) \cdot C_{direct} \\ R_{1000} = (p_{1000} - p_{5000}) \cdot C_{1000} \\ R_{5000} = p_{5000} \cdot C_{5000} \end{cases}$$

Where R is the partial risk, p is the probability, and C are the consequences. Here, the probability of the next scenario is subtracted to get the probability at which a scenario is reached, while the next scenario is not exceeded (e.g. Bründl et al. 2009). The total risk is then the sum of all partial risks:

$$R_{total} = R_{direct} + R_{1000} + R_{5000}$$

Finally, the consequences corresponding to the probability of rupture assuming an equivalent risk are obtained as follows:

$$C'_{direct} = \frac{R_{total}}{p_{direct}}$$

4. Results

4.1 Stiksmoen unstable rock slope – main features

The unstable rock slope developed between ~120 m and ~30 m a.s.l., in phyllite. The backscarp is well developed and presents a maximum opening of ~9 m in the northern sector but an unknown depth because it has been filled with blocks falling from the backscarp wall and with boulders removed by the locals from the glaciomarine deposits located on Sletta. The northern flank of the unstable rock mass is well developed and free, while the southern one is moderately developed and partially covered with a boulder field. The front of Stiksmoen is characterized

by a cliff where small collapses in the form of rock falls occur. The toe of the unstable rock mass is covered by a block field that extends down to Vikjavegen (Figure 7; Figure 8). The sliding surface is not clearly visible on the slope, and it is considered to cut the slope close to where graphite material was observed (Figure 9).
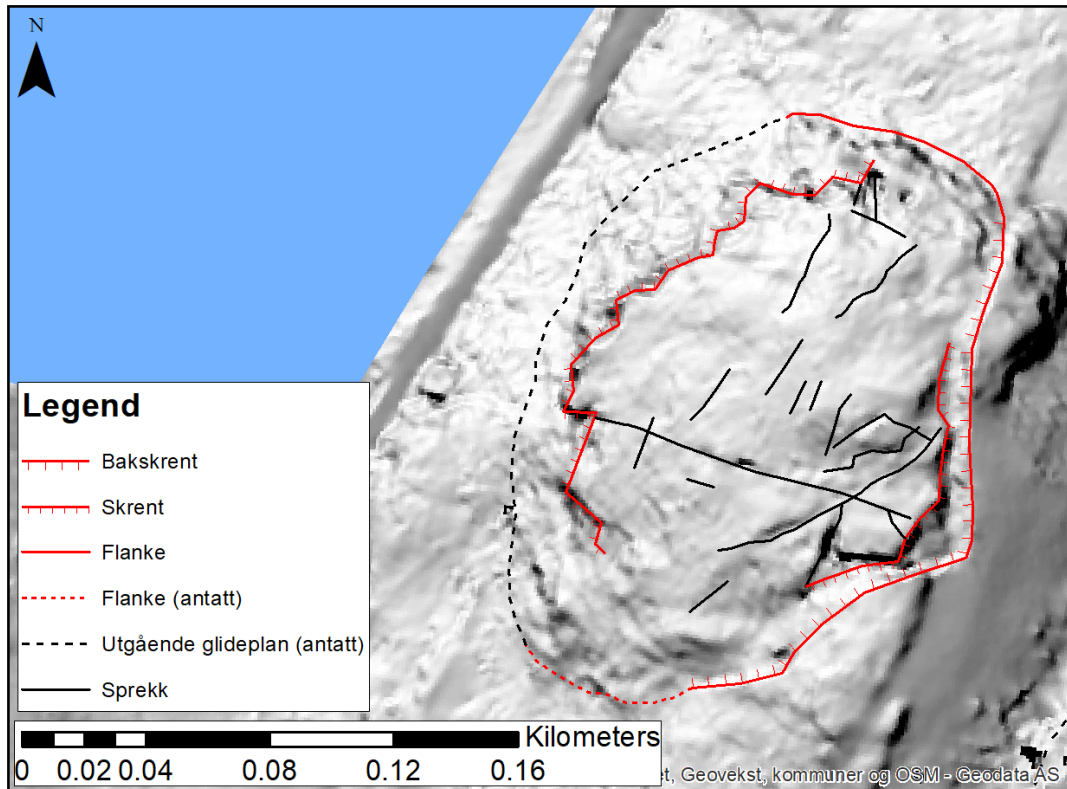
Figure 7. Hillshade map with mean lineaments observed on Stiksmoen.
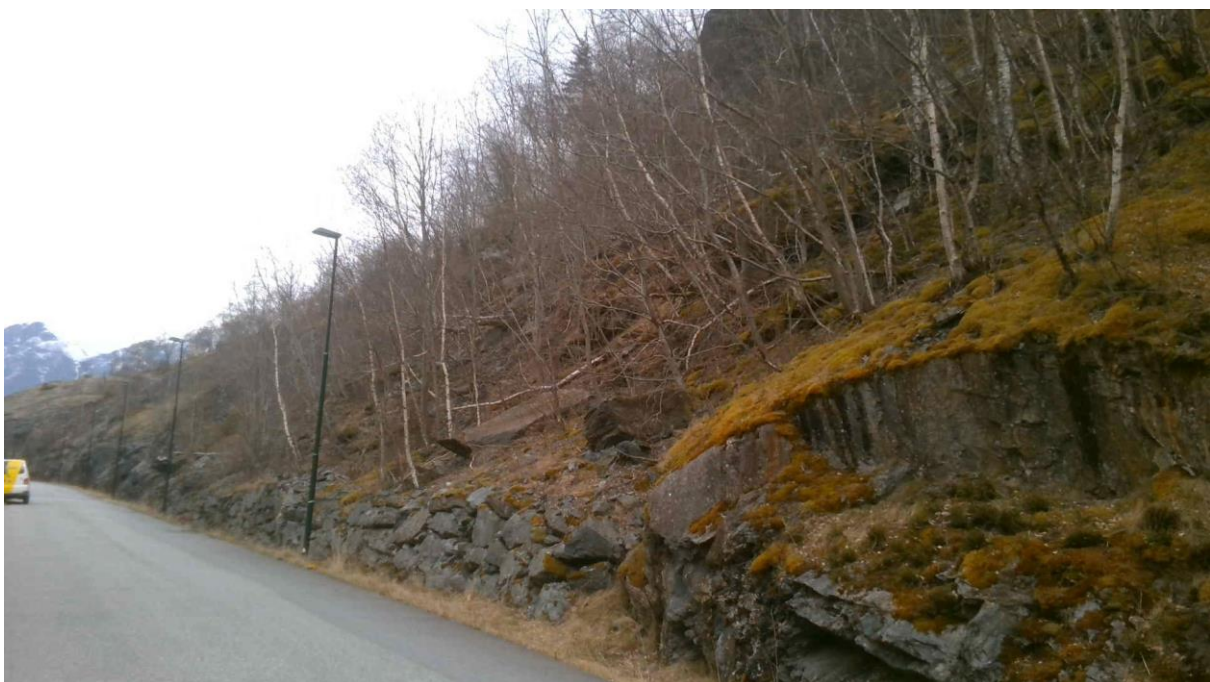
Figure 8. View to the north along Vikjavegen. Retention wall and accumulation of blocks detached from the frontal part of the instability.

16
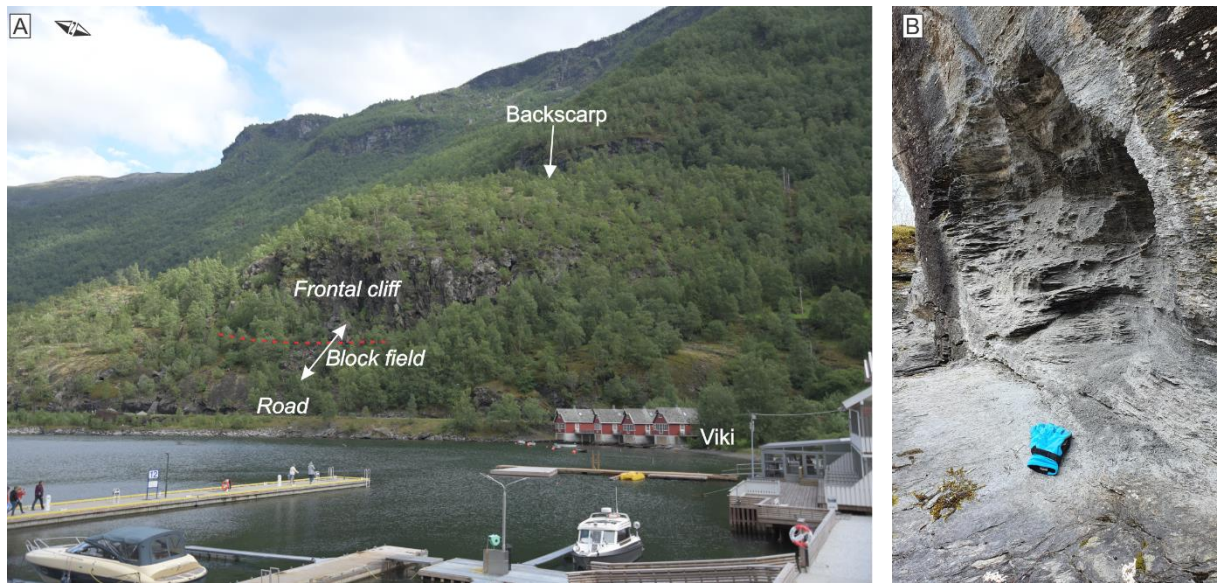
Figure 9. View of Stiksmoen from Flåm. The dashed red line marks the approximately location of the toe of the instability. B) Graphite rich lenses in the southern limit of the instability, close to the location of the toe.

Regarding the fracturing of the rock mass, we observe differences from the upper to the lower part. The upper part of the instability shows a higher degree of fragmentation and opening of cracks. In this zone, open cracks 10-15 m deep separate blocks of around 50-100 m^2. Fewer open cracks are observed on the surface in the central and frontal (lower) parts of the instability.

4.2 Mechanism of deformation – Structural analyses

The foliation of the phyllites is highly variable but has a general trend dipping towards the west. Foliation is strongly folded, and due to developed crenulation cleavage, it is often difficult to measure foliation planes (Figure 10).

Figure 10. Small scale folds affecting the phyllites in the southern part of the instability. (Picture: Martina Böhme).

In the field we observed at least two major orientations of foliation that cross each other, one forming a potential sliding plane (average orientation 262/39) and the other one constituting the lateral limit (average orientation 218/63). However, on the stereogram it gets obvious that all foliation poles concentrate along a great circle and can thus be attributed to the same fold geometry with a fold axis oriented approximately 291/35 (Figure 12 and Figure 13). This is similar to the displacement vector obtained from dGNSS (305/40), indicating an influence of different foliation orientations on the sliding mechanism.

The fracture set that is best developed is dipping steeply into the slope with an average orientation of 114/57. Another set, less developed, has a very similar trend but is vertical (average orientation 308/90; Figure 12 and Figure 13). The backscarp is quite complex and follows different structures over its length. In the northern part, it is clearly developed along steeply dipping foliation planes (Figure 11; average orientation 260/58) while following multiple fracture planes further south.

Figure 11. View towards the southeast. Backscarp developed along the foliation.

A kinematic analysis indicates planar sliding as well as wedge failure as probable failure mechanisms (Figure 12 and Figure 13). For both sliding mechanisms, foliation would form the sliding plane(s). For planar sliding, the general trend of foliation is most important. Whereas for wedge failure, sliding would additionally also take place on different foliation orientations, mainly as a lateral constraint. Planar sliding is consistent with the homogeneous degree of deformation of the rock mass. The unstable rock slope does not present specific sectors with higher deformation, which is seen on instabilities where the angle of the sliding surface changes.
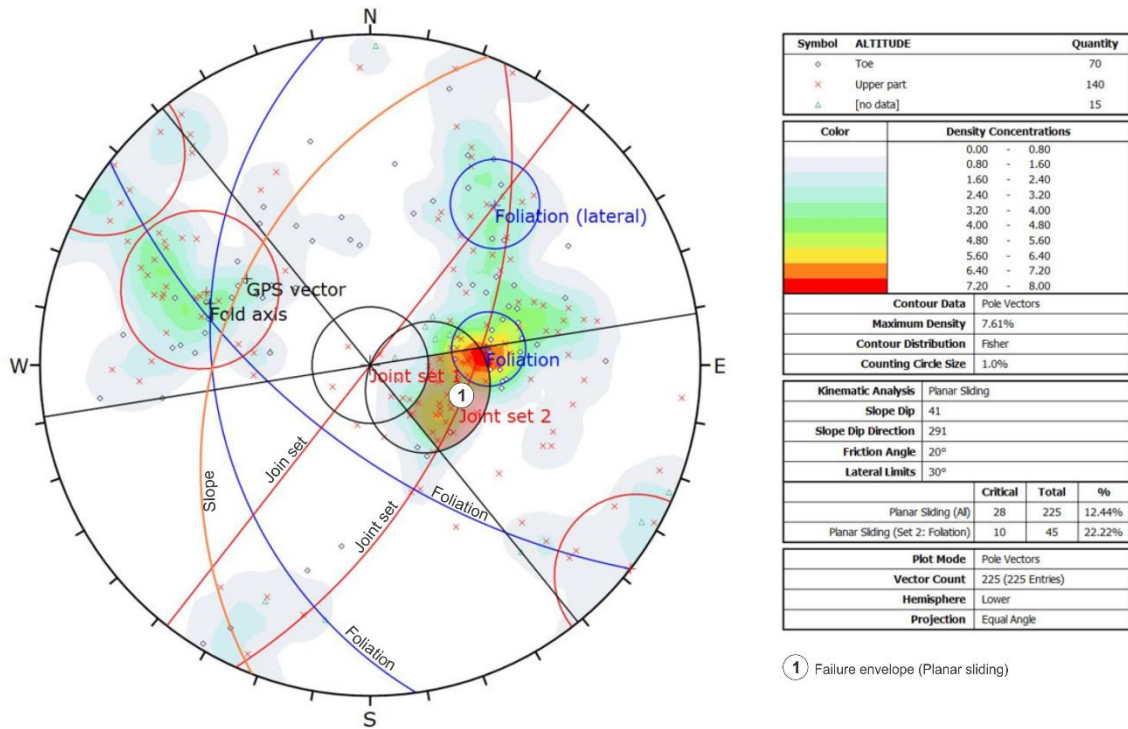
Figure 12. Kinematic analysis. Planar failure.
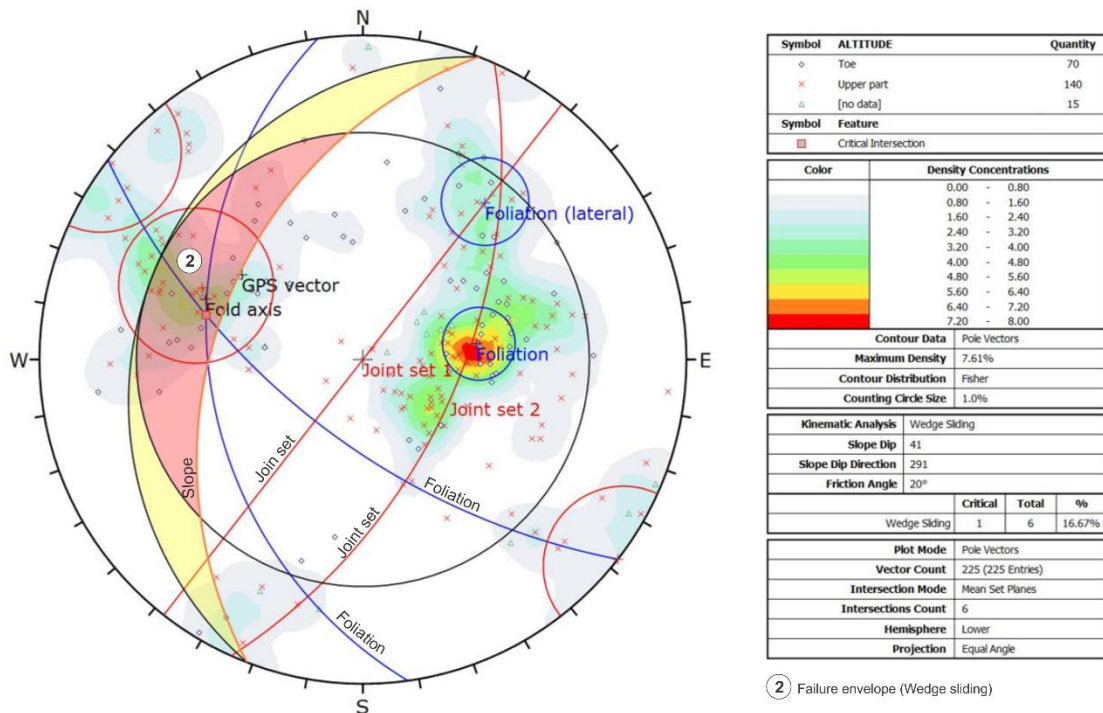
Figure 13. Kinematic analysis. Wedge failure.

Grimstad (1987) proposed sliding along foliation planes dipping ca. 30° towards the fjord. In our work we propose an irregular sliding surface developed along the foliation, dipping towards the fjord, and with steps formed by the breaking up of minor-scale folds (Figure 10).

4.3 Volume of the unstable rock slope

The unstable rock slope extends over 0.02 km^2. Its thickness is higher in the central-northern part, where it reaches ca. 30 meters (Figure 14). The reconstructed sliding surface is located approximately 70 above the Fretheim tunnel (Figure 15). The computed volume is 397 000 m^3.
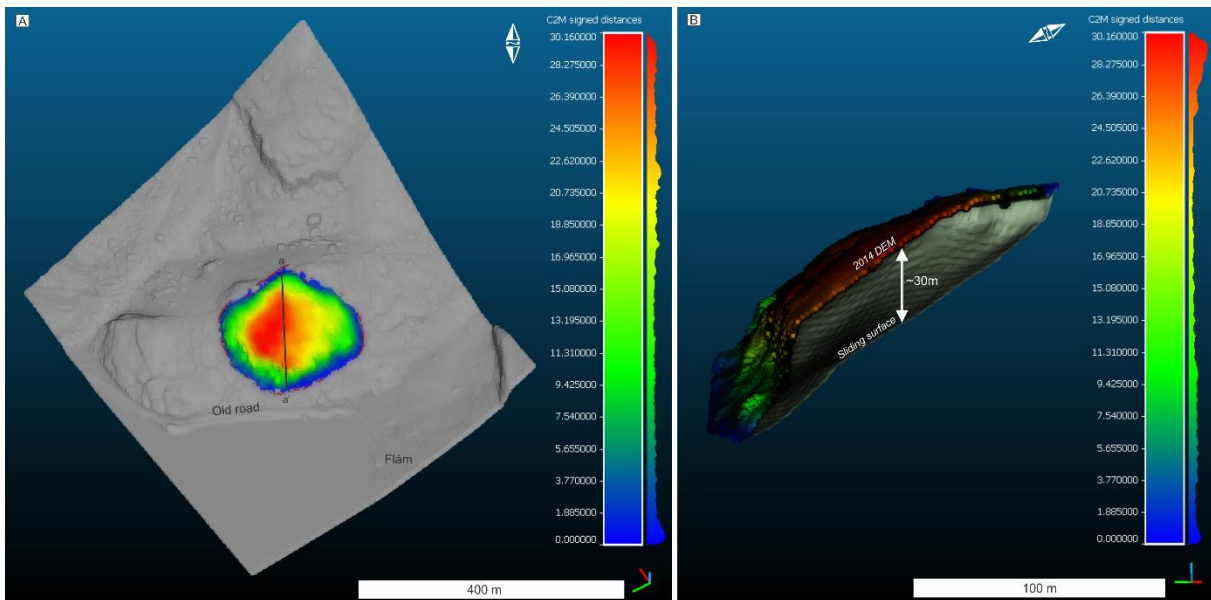
Figure 14. C2M (Cloud to Mesh) distances computed between the 2014 DEM and the reconstructed sliding surface show thicknesses of up to 30 meters. A) View of the 2014 DEM (grey colours), the thickness of the unstable rock slope (blue to red colours), and the location of slice shown in figure B. B) 3D profile showing the 2014 DEM with C2M distances, and the shape of the sliding surfaces.
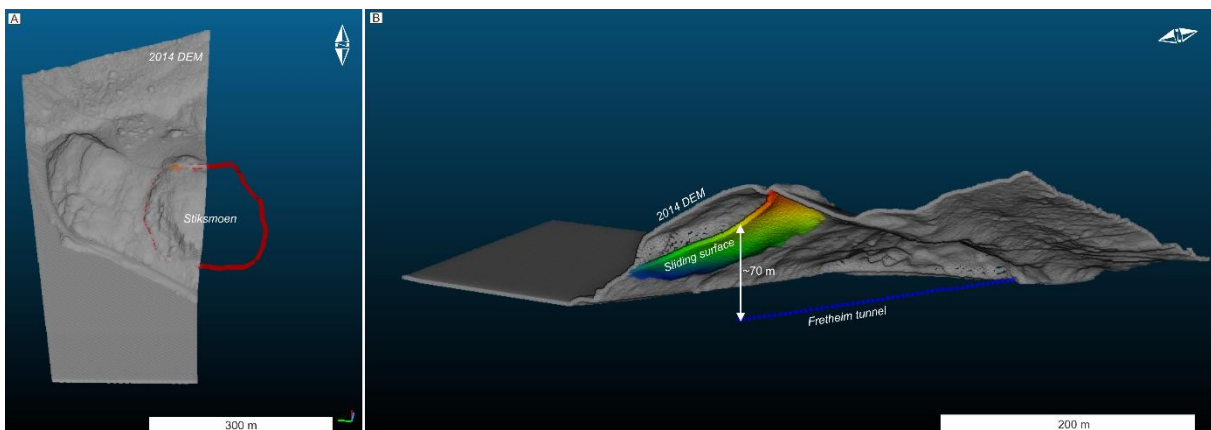
Figure 15. A) View of the 2014 topography and the limits of the unstable rock slope. The 2014 is cropped to the slice limits showed in figure B. B) Down-up 3D View of the 2014 topography (slice showed in A), the reconstructed sliding surface, and the path of Fretheim tunnel.

4.4 Displacement rates

The displacement rate of Stiksmoen has been determined through different in situ and remote measurement methods. The following sections indicate the time of measurements and summarize the main results.

4.4.1 Extensometers

Two extensometers were installed in 2016 in the backscarp (see location in Figure 5). The displacements measured along the years show a constant trend. The northern one shows a displacement rate of 1.5 cm/y and the southern one 0.9 cm/y (Figure 16).
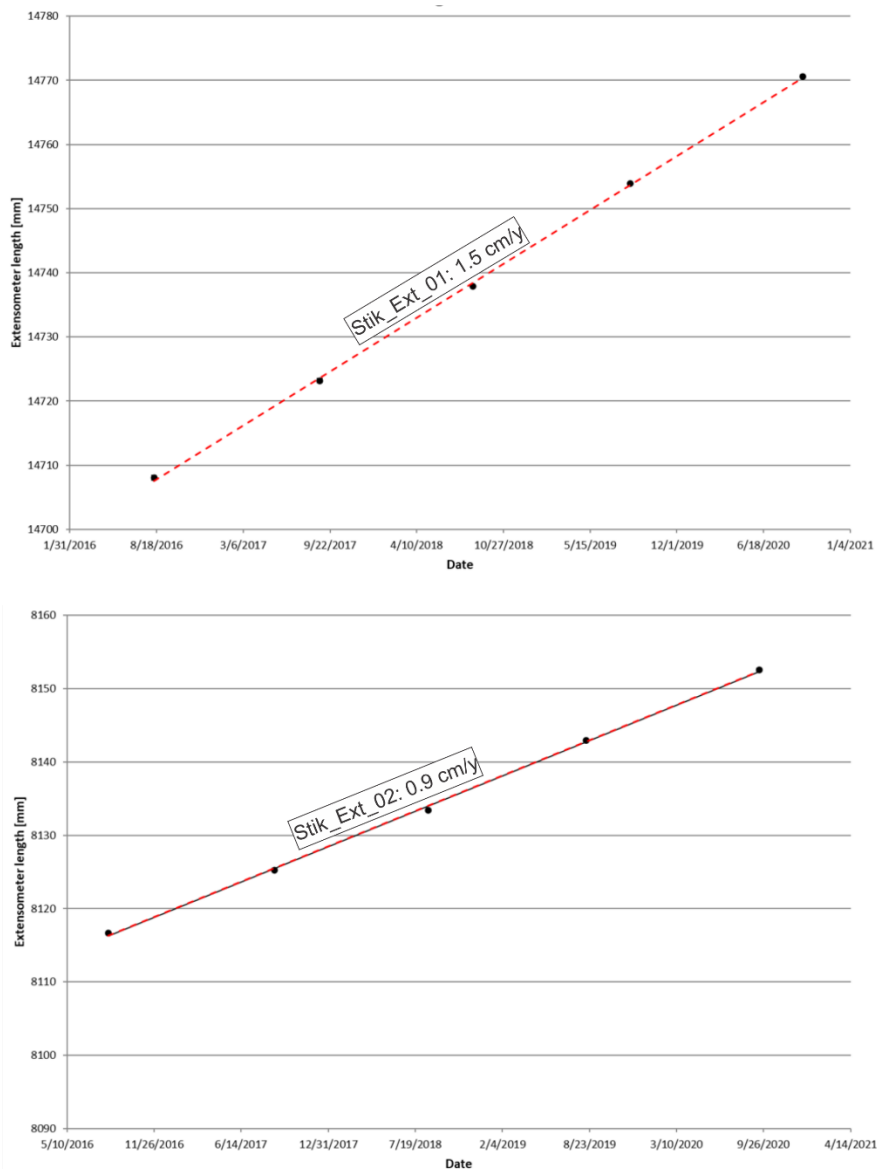
Figure 16. Displacement rates measured with extensometers. Orientation extensometer 1: 244/01. Orientation extensometer 2: 319/08.

4.4.2 Differential Global Navigation Satellite System (dGNSS)

Since 2016, Stiksmoen has been annually measured using this method. The measuring point, installed on the unstable rock mass (Figure 17 and Figure 18), shows a statistically significant vertical and horizontal displacement. It is observed a constant trend in displacement between 2016-2020, both vertical and horizontal. The displacement rate measured is 24.6 mm/y with a vector oriented 305/40 (Figure 19).

Figure 17. Location of the dGNSS antenna in Stiksmoen.
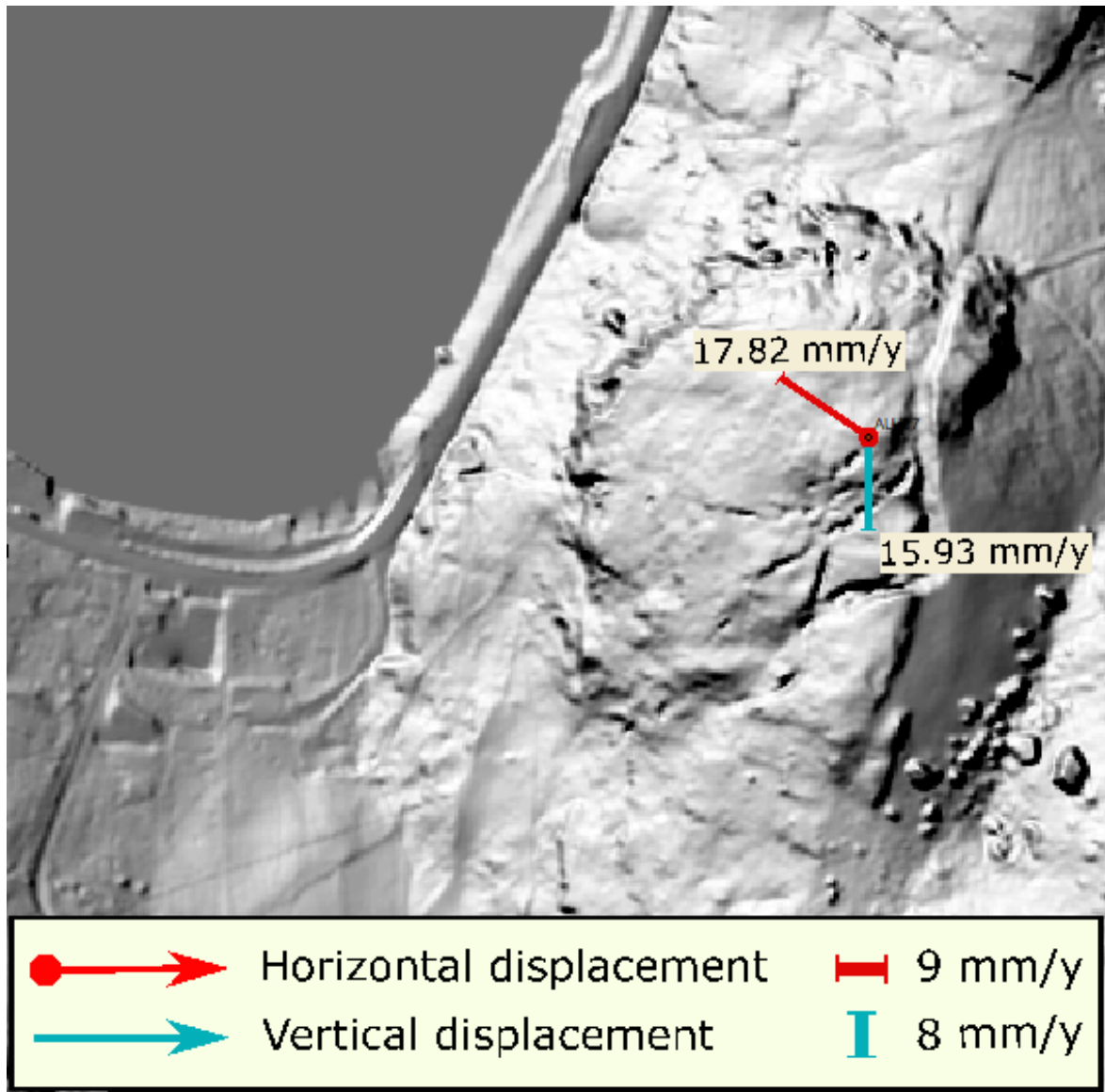
Figure 18. Hillshade with location of the dGNSS point and the corresponding vectors of displacement.
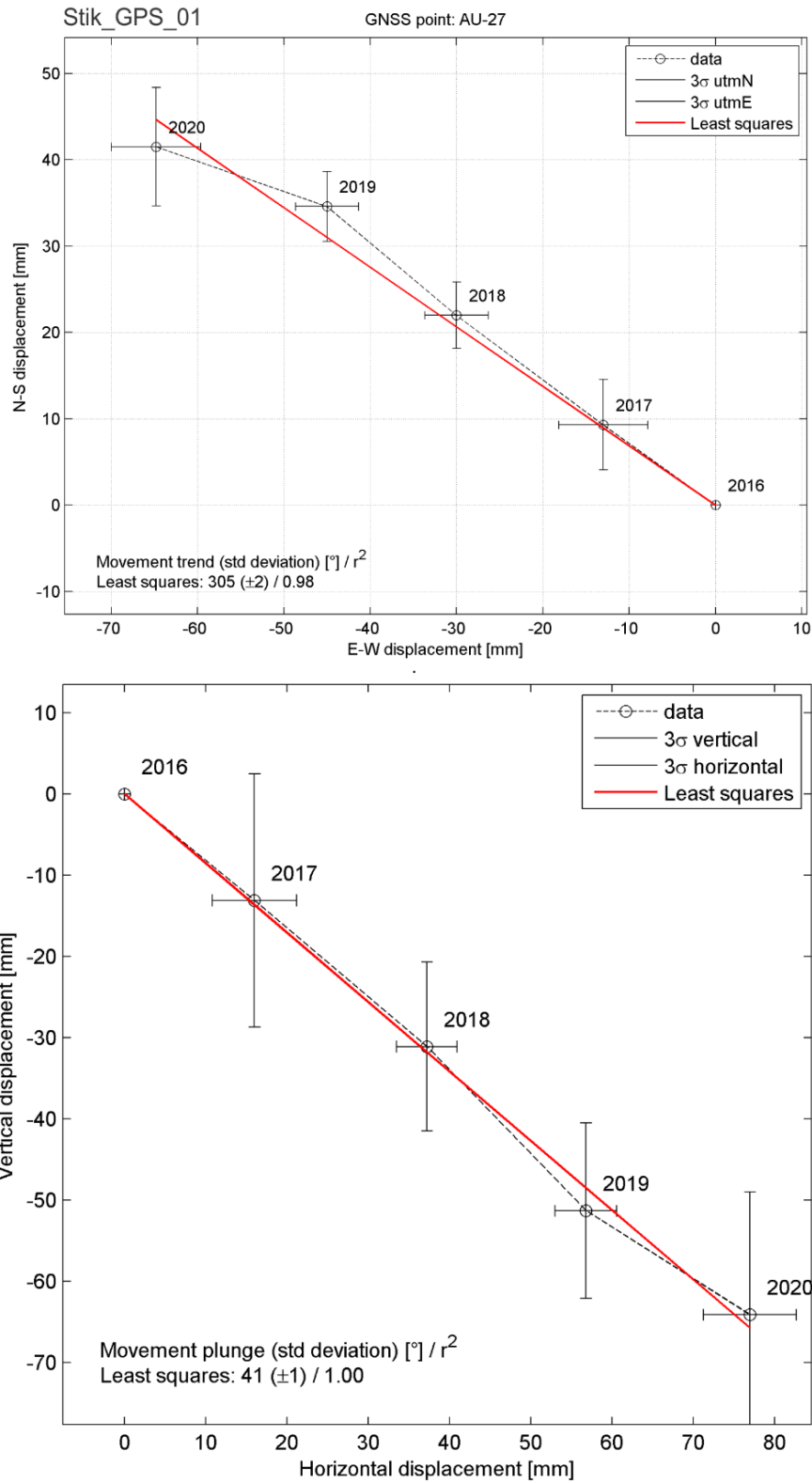
Figure 19. Displacement rate measured with dGNSS.

4.4.3 Satellite-based radar interferometry (InSAR)

Because of the vegetation coverage, and geometry of the area there is poorly coverage of InSAR data (Figure 20). However, some data exists from the Sentinel-1 descending radar (2016-2019)

for the upper-central part of the unstable rock mass, in the vicinity of the dGNSS point. The measurements show a displacement rate of 24.5 mm/y along the line-of-sight vector, oriented 281/37 (Figure 21). This is comparable to the displacement rate (24.6 mm/y) measured with dGNSS. The dGNSS displacement also indicates that the displacement direction is like the line-of-sight and InSAR displacement can thus be assumed to be of good quality.
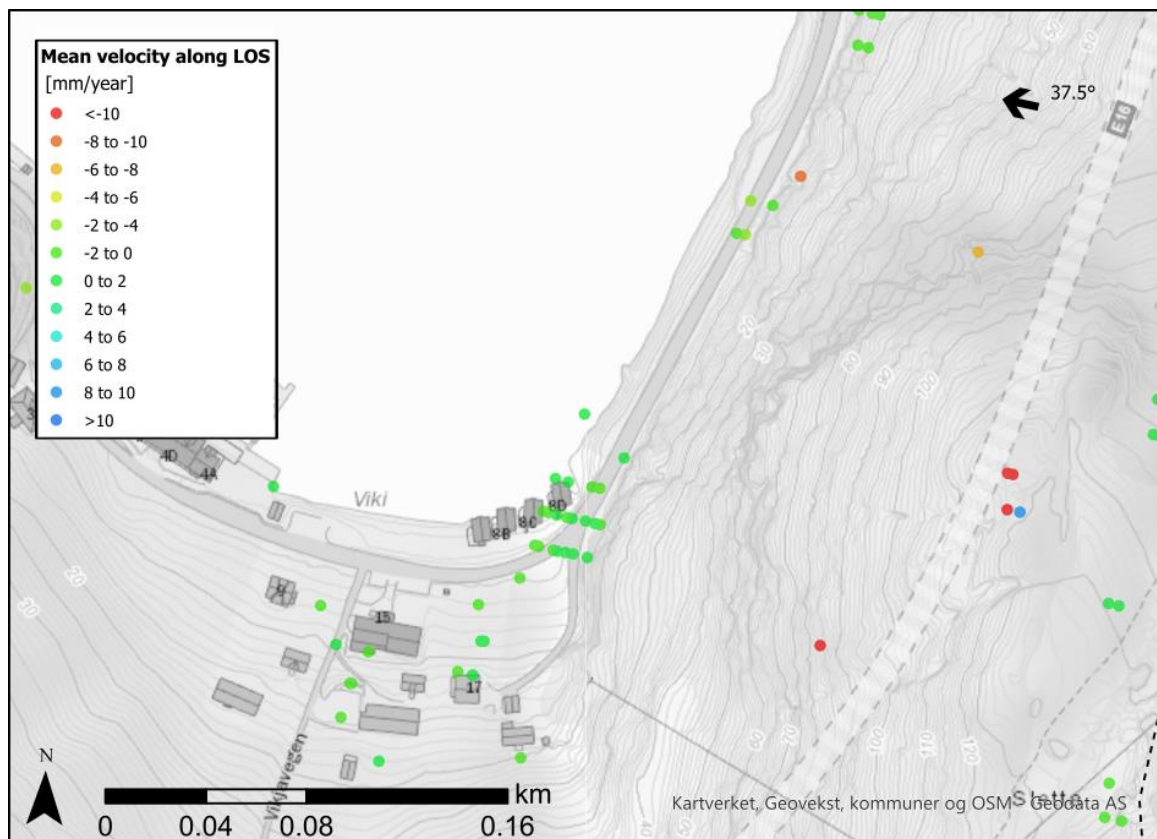
Figure 20 InSAR mean velocity [mm/year] along line-of-sight (LOS) in descending geometry (orientation of black arrow: LOS azimuth angle, label: LOS incidence angle).
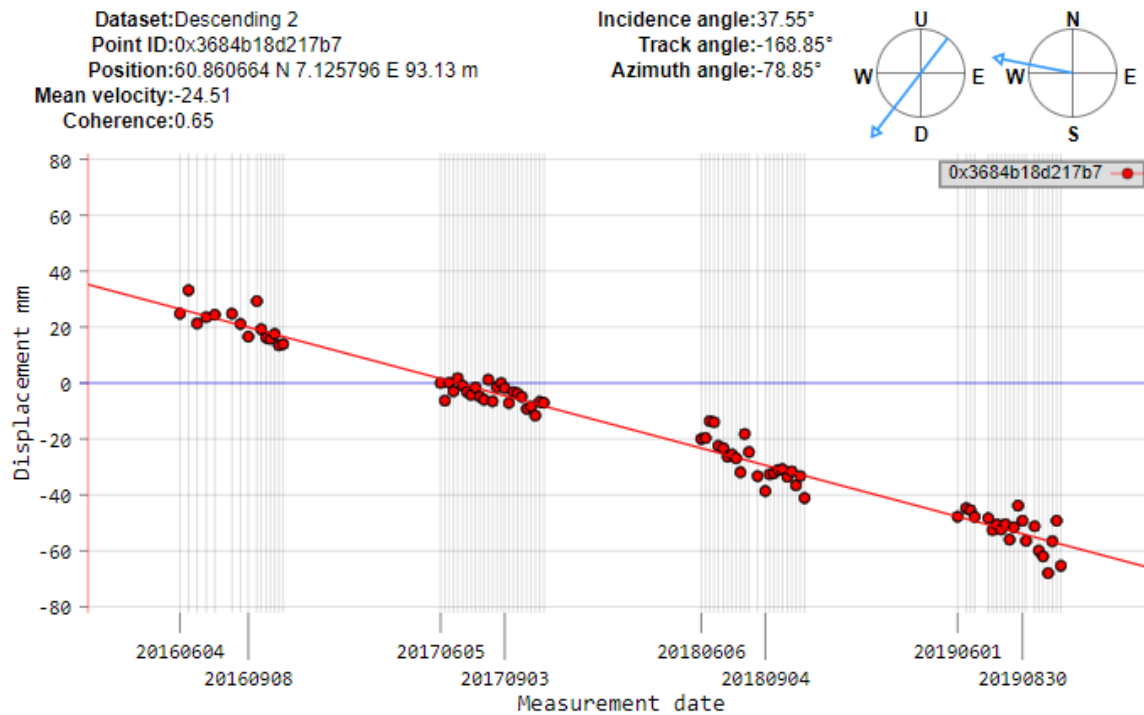
Figure 21 InSAR time series of points on the upper central part of Stiksmoen, showing a yearly displacement of 24.5 mm.

4.4.4 Ground-based radar interferometry (GBInSAR)

NVE has carried out measurements with GB InSAR in 2018 and 2019. The unstable rock mass is quite vegetated in the upper and central part but not the frontal part, where the visibility of the radar was considered good enough to measure displacements. The measurements in 2018 are at 3-month intervals and in 2019 the measurements were 45 days apart. The displacement measured in both field campaigns is similar and in the order of 0.8-2.5 cm/y. The data suggest that a central part is moving faster than both flanks. The scattered datapoints on top of the forested block are not trustworthy (noise from the vegetation).
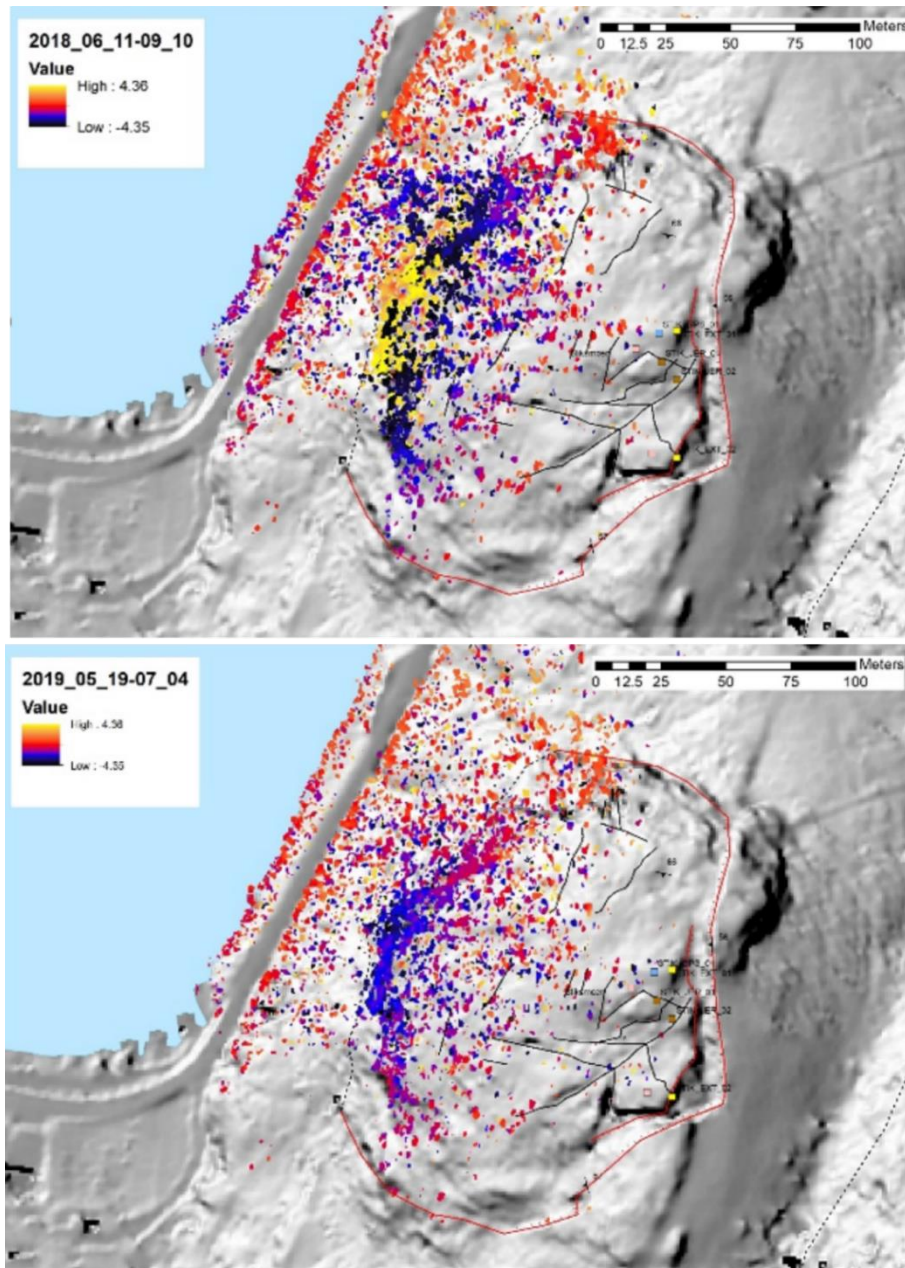
Figure 22. Hillshade maps and displacement rates measured with GB-InSAR. Upper part: results of the measurements in 2018. In yellow the area with phase wrapping (meaning displacement is higher than 4.4 mm). Lower figure: results of the measurements in 2019 (reference: NVE internal report).

4.5 Geologic model

Displacement rates measured in the upper part of the unstable rock mass with dGNSS and satellite InSAR are very similar to those measured with the GB-InSAR in its frontal part. The dGNSS displacement vector is oriented ca. 305/40. The similar displacement rates in the upper and lower-frontal parts suggest a quite homogeneous displacement of the rock mass. The structural conditions and the dGNSS vector point out to a rupture taking place along a stair-step like surface cutting through the tight fold axis as well as through soft graphite rich lenses, as

observed in other parts of Stampa (Böhme et al., 2013; Blikra et al., 2013). The sliding surface cuts the slope between 30-40 m a.s.l., where a zone of graphite rich lenses is observed.

In sum, the development of the unstable rock slope Stiksmoen is the result of a complex interaction between foliation with variable orientation and different joints sets, where graphite layers seem to play an important role in facilitating its development and favouring its displacement (Figure 23).
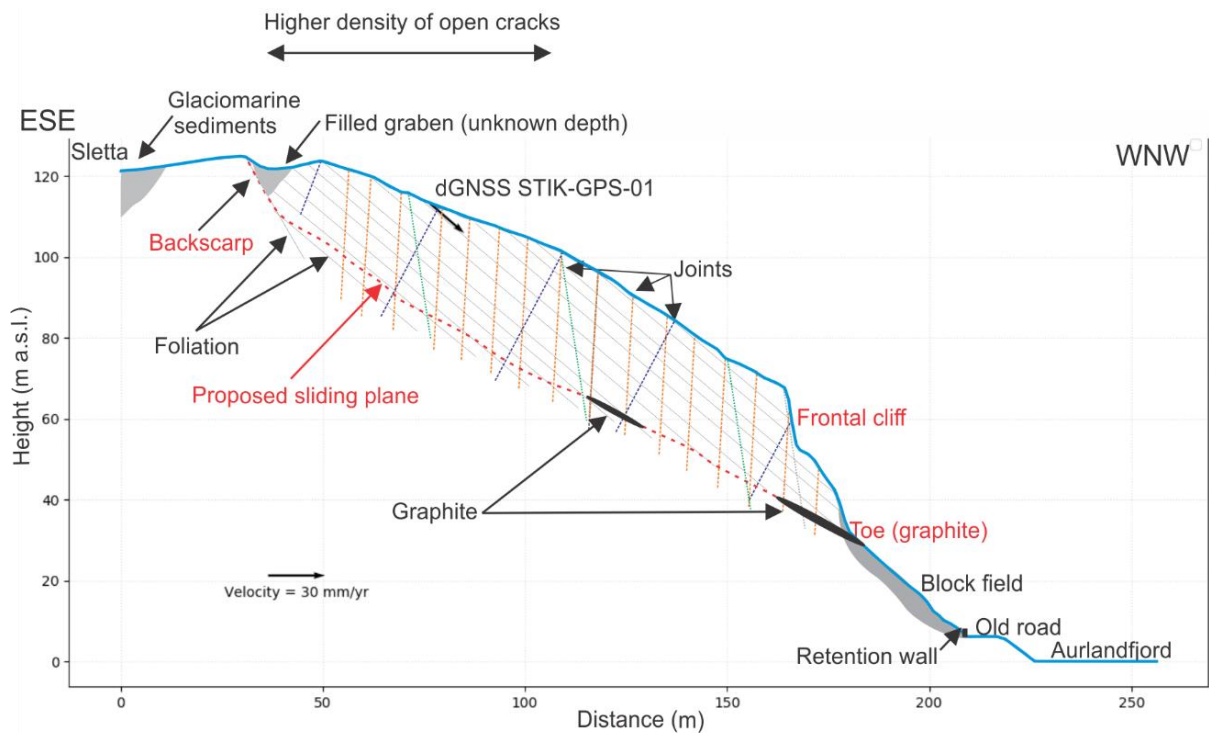
Figure 23. Conceptual geological model of Stiksmoen.

4.6 Run-out analysis

The dynamic modelling of Stiksmoen showed that the collapse of ca. 0.4 million m^3 would imply a large volume of rocks reaching the fjord, in the vicinity of Flåm (Table 3 and Figure 24). The main propagation direction of the rock mass is WNW, but the southern part of the unstable rock mass would propagate on land towards Viki. The shortest run out (330 m) is observed in the T7 model and the longest one in the T4 model (413 m; Table 3). The modelled velocity of the rock mass when impacting the water ranges between 13.8 to 15.7 m/s.

Table 3. Volume entering the fjord and average velocity at the impact with the water for the 10 models done with DAN3D.

Model ID	Volume into the fjord (m^3)	Average velocity (m/s) at 0 m	Maximum run out distance (m)
T7	122004	13.8	330
T3	123609	15.4	369
T1	160732	14.8	376
T9	172572	14.3	360
T5	183809	14.1	366
T2	200665	15.2	380
T10	245012	13.9	371
T6	246617	13.9	384
T4	277520	15.7	413
T8	284142	14.4	395
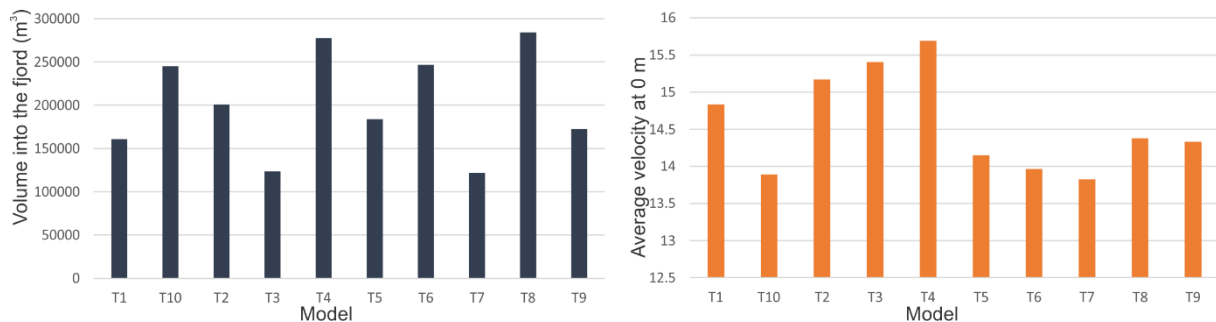
Figure 24. Histograms showing the distribution of volumes into the fjord and average velocity for the considered models.

In the model T4, the propagation indicates the rock mass reaching 26 m b.s.l. Models T4 and T8 show the largest volumes falling into the water, but the highest average velocity at the impact on the water is observed in model T4. Model T7 resulted in the smallest volume propagating into the water and lowest velocity at the impact with the water. Model T2 represents an intermediate scenario of these two extremes. In this scenario ca. 200 000 m^3 of rocks will enter the fjord at an average velocity of ca. 15 m/s (Table 3; Figure 25; Figure 26), spreading over 0.11 km^2.
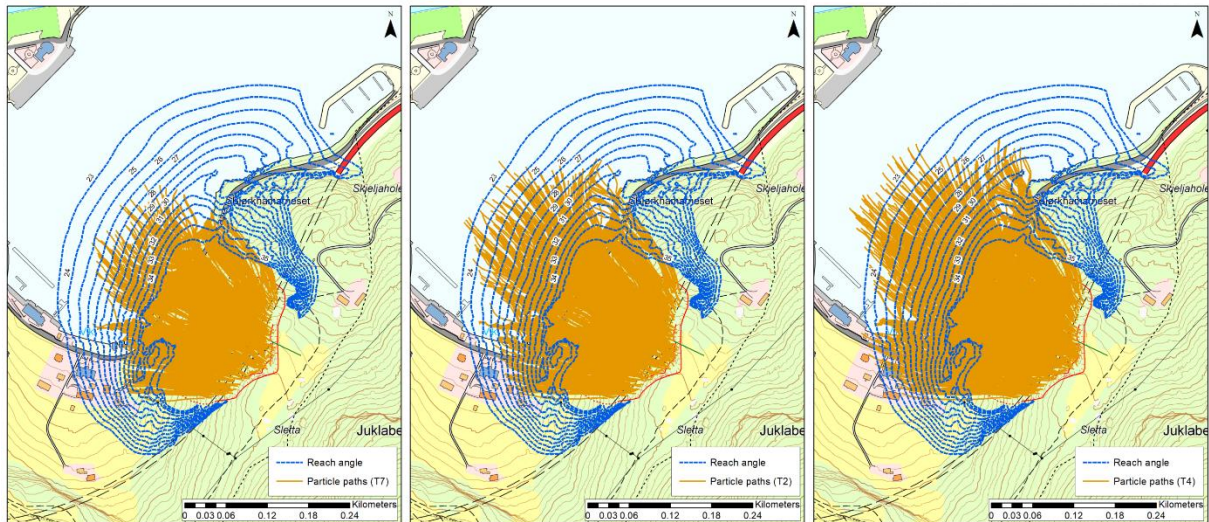
Figure 25. Propagation maps for the T7, T2 and T8 models. The path of the particles in the source area and the reach angles are shown.

The intermediate scenario (T2) shows that shortly after the collapse of the rock mass most of the material has propagated into the fjord (Figure 26).
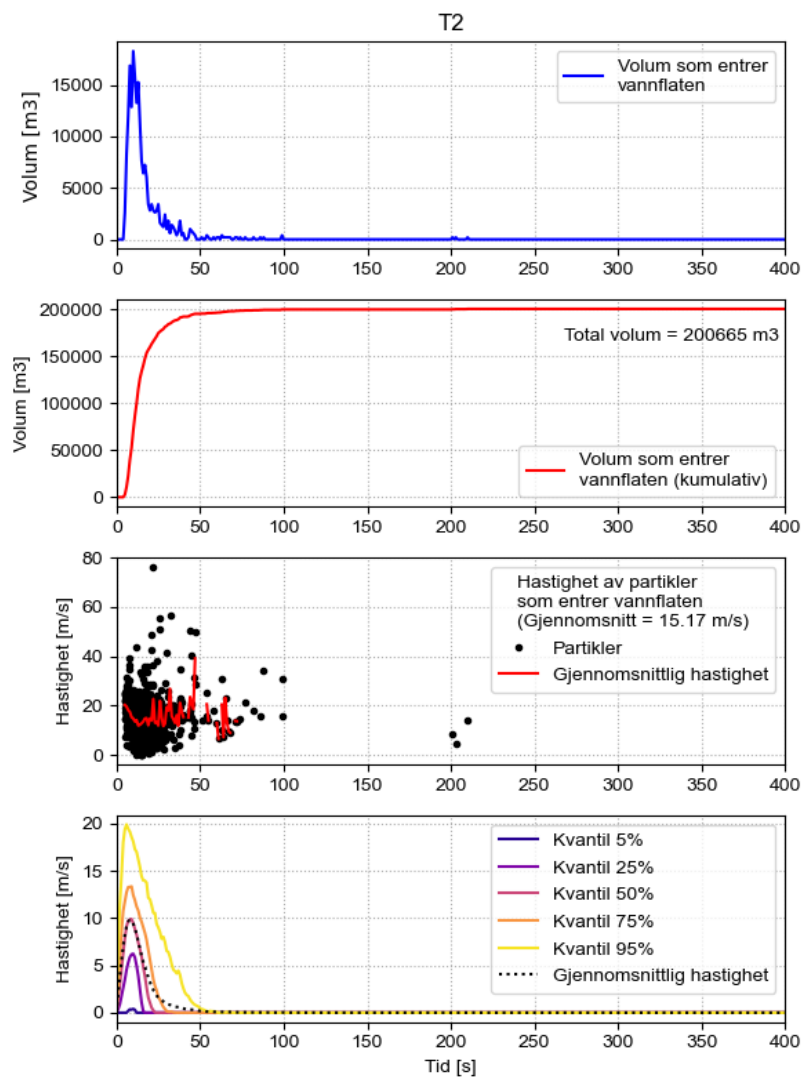
Figure 26. Scenario T2. Volume entering the fjord and velocities of particles when entering the fjord.

4.7 Displacement wave analysis

The analysis of the displacement wave was carried out by NGI. Details on the analysis can be found in Glimsdal (2022).

4.8 Hazard and risk assessment

In this section we present the results of the hazard and risk assessment based on the NGU methodology (Hermanns et al., 2012).

4.8.1 Hazard classification

The hazard level is estimated based on the assessment of 9 criteria related to the degree of development of the instability, the kinematics, dynamics and on the assessment of precedent events in the area (see **Appendix 1**). Below we present the considerations used for the ranking:

1) **Backscarp**: Well developed backscarp. Max. opening of ca. 9 meters, unknown depth (depression filled with blocks from the unstable rock mass, glaciomarine sediments removed from Sletta, and trash). Developed in the central and northern part along foliation.

2) **Potential sliding surface**: Developed mainly along foliation, breaking through along axis of small folds. Graphite layers at the toe of the unstable rock mass. Dip: 30-40 degrees.

3) **Flanks**: The northern flank is free. The southern flank is less developed and in parts covered by scree material.

4) **Kinematic analysis**: Complex planar sliding along foliation that dips 30-40 degrees towards the fjord. Structural measurements indicate planar sliding as most probable mechanism, but wedge failure is possible. The NGI report proposes a kind of planar sliding along foliation that dips 30-40 degrees towards the fjord.

5) **Morphologic evidence on the lower limit**: The location of the lower limit is relatively well constrained. Graphite horizons observed, slope break and geophysical survey indicating it.

6) **Displacement rates**: Between 0.9 and 1.5 cm/y measured with extensometers. dGNSS, InSAR and GB-InSAR of around 2.5 cm/y. Category 1-4 cm/y in the NGU classification system but with some weight to the class 0.5-1 cm/y.

7) **Acceleration**: The available information cannot be used to confirm or rule out acceleration. Current measurements seem to be higher than those measured by NGI with extensometers. However, measurement methods were different and took place on

different parts of the unstable rock mass. NGI placed most of the bolts for measuring with extensometers on the upper sector presenting most of the fragmented blocks. Therefore, they have measured compartments and may not cover the entire displacement.

8) **Rockfall activity**: More rockfall activity than in the surroundings. Retention wall along the road.

9) **Past events-postglacial**: The occurrence of past events is well known in the eastern slope of Aurlandfjord between Stampa and Ramnanosi. A small collapse, immediately north of the instability, is observed in bathymetric data. It is well preserved and only partially buried with sediments.

The hazard level for Stiksmoen is 8.7, which correspond to a high hazard level.

4.8.2 Consequences

A total collapse of this unstable rock slope would result in rocks propagating towards the fjord and the WSW (Figure 27). This could lead to consequences related to the direct impact of the rock mass but also because of the triggering of a displacement wave. The consequences in this report relate only to the potential losses of lives and are divided as 1) related to the main impact, 2) related to the displacement wave.

1) *Direct impact area*: there is 1 house with 2 residents in the run-out area. In addition, there are 4 cabins and 1 garage. For each cabin, the standard values are: 1 person minimum, 3 persons average and 6 persons maximum with an estimated exposure of 25%. For other types of buildings such as shed, garages, houses for animals, etc. no persons are considered. In total, this results in between 4 to 8 potential fatalities, in the direct impact zone, in case of a total collapse of Stiksmoen.

2) *Displacement wave*: most of the computed consequences belong to the tourists visiting Flåm, since just few permanent residences are in the hazard zones for displacement wave (see Appendix 1). No fatalities are considered for buildings with no people living on or with long stays (sheds, garages, boathouses, houses for animals). Flåm receives ca. 1 million tourists per year. The highest incidence occurs between April and October. On average ca. 609 fatalities could occur because of the displacement wave related to the total collapse of the unstable rock mass considering the 1/5000 hazard zone.
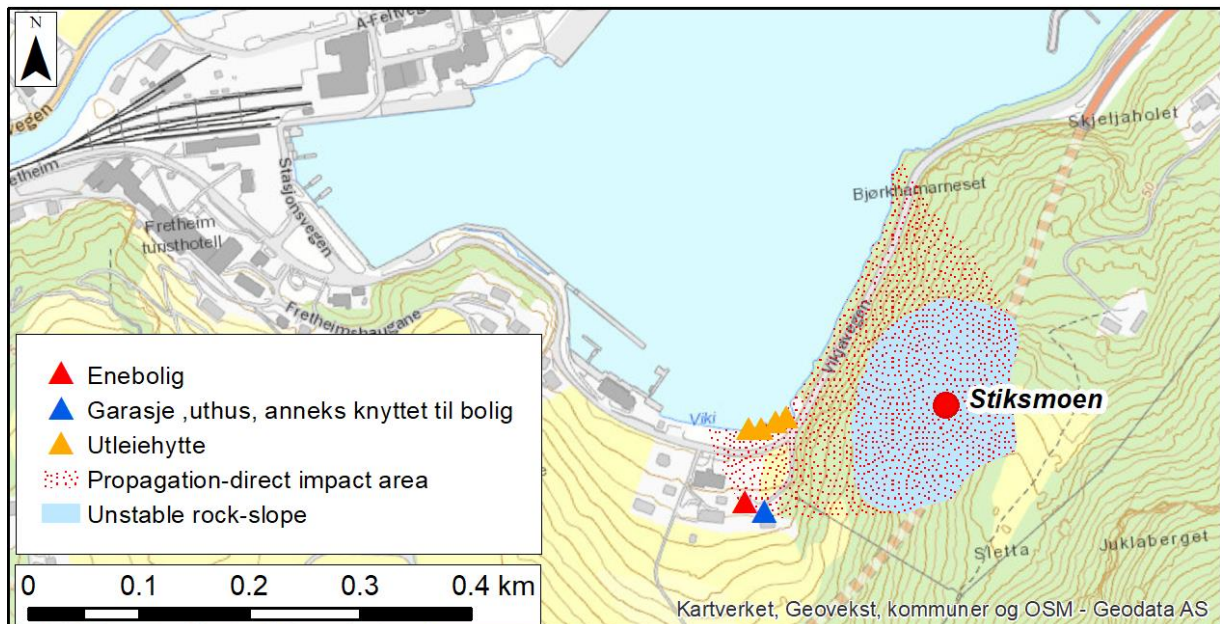
Figure 27. Consequences on the direct impact zone.

4.8.3 Risk classification

The hazard score (8.7) corresponds to a probability of 0.00348 and a return period of 287 years.

The partial risk for the different scenarios considering the average consequences is as follows:

$$\begin{cases} R_{direct} = 0.0062 \\ R_{1000} = 0.927 \\ R_{5000} = 0.368 \end{cases}$$

The total risk is then 1.3 death/year, which corresponds to 374 deaths with the failure probability of $3.48*10^{-3}$. This probability and consequence are then plotted inside the risk matrix. See Ap.Figure 3 for more details.

The contribution of the 1/1000 scenario to the total risk is the largest, while the one of the direct scenario is the smallest. This is due to the procedure used for the calculation of the probability explained in section 3.6.2. and the relatively similar frequency for the direct and the 1/1000 scenario, in contrast to their large difference in consequences.

The result of the risk assessment is presented in Figure 28. According to our analysis Stiksmoen is classified as a high-risk site.
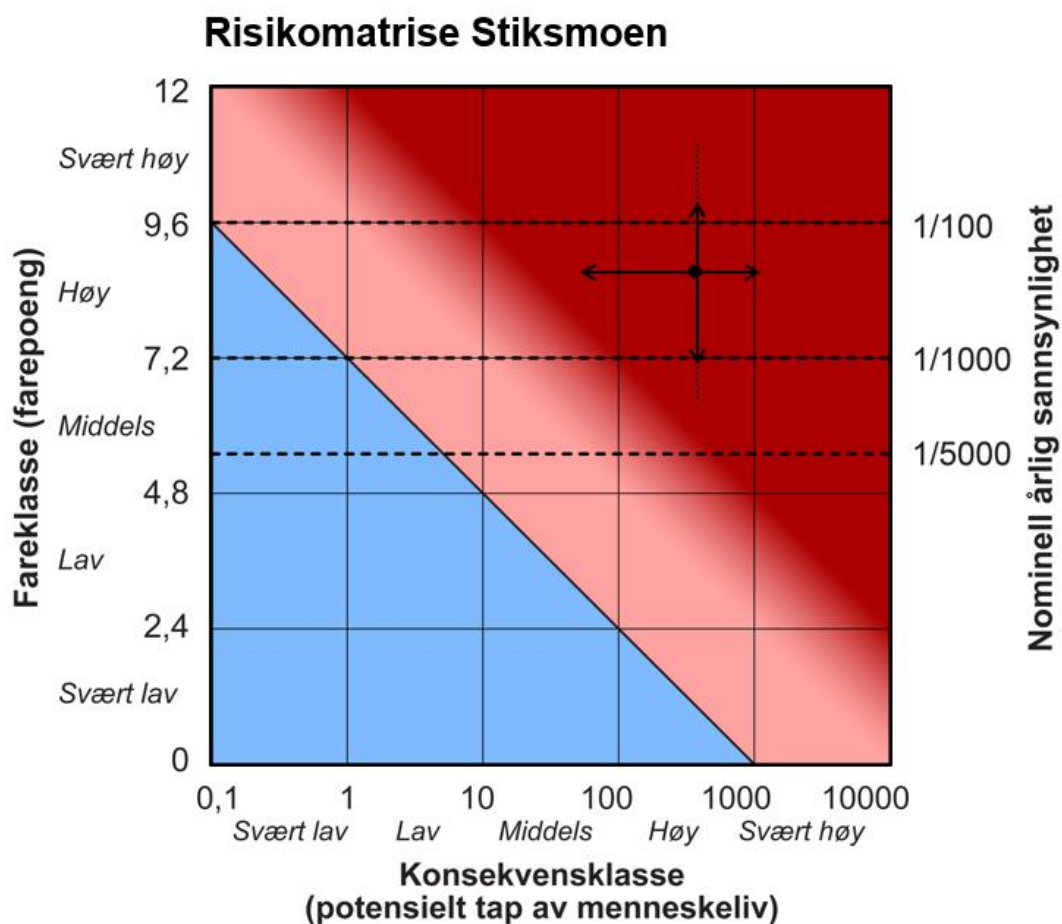
Figure 28. Risk matrix for Stiksmoen considering direct and indirect consequences.

5. Discussion and conclusions

This report presents an analysis of the current situation for the unstable rock slope Stiksmoen in Aurlandfjord (Flåm municipality). Our work includes the assessment of the morphological and structural conditions of the site, the modelling of the sliding surface, the computation of its displacement rates, the modelling of the rock mass propagation, and finally the assessment of the hazard and risk level.

Stiksmoen (ca. 397 000 m^3) is a well-developed unstable rock slope with displacement up to 2.5 cm/y. The fact that the measured displacement rates with dGNSS, and satellite and GB-InSAR in the upper and frontal part are very similar, point to a rock mass displacing quite uniformly. This and the results of the kinematic analysis indicate planar sliding as the most likely failure mechanism. A single scenario is considered for Stiksmoen based on its aforementioned conditions. Recently measured displacement rates are higher than those indicated in reports from the 70-80s (Grimstad 1987). However, the use of different measurement techniques and the fact that in the 80s the measurements were done on the highly

detached blocks from the upper part of Stiksmoen does not allow comparison and acceleration on the displacement of the rock mass cannot be verified.

A sudden collapse of Stiksmoen would produce a rockslide partially propagating into the Aurlandfjord, in front of the Flåm harbour, with the worst-case scenario having a run-out of more than 400 meters, which corresponds to an angle of reach of 22-23°. It must be pointed out that for the volume of Stiksmoen, the empirical relationships based on an inventory of landslides (Scheidegger 1973) would indicate angles higher than 23°. However, the inventories are biased since they only consider few cases of landslides with subaerial and underwater propagation.

The direct impact of the rock mass and its related displacement wave could cause hundreds of fatalities. The high hazard and the high consequences result in a high risk for the unstable rock-slope Stiksmoen. It must be pointed out that our assessment does not include secondary slope destabilizations caused by the propagation of the rock mass or the displacement wave in natural or human-modified (landfills) terrains.

6. Acknowledgements

7. References

Blikra, L.H., Braathen, A., Anda, E., Stalsberg, K., and Longva, O., 2002. Rock avalanches, gravitational bedrock fractures and neotectonic faults onshore northern West Norway: Examples, regional distribution and triggering mechanisms. NGU report no. 2002.016.

Blikra, L.H., Longva, O., Braathen, A., Anda, E., Dehls, J.F., and Stalsberg, K., 2006. Rock Slope Failures in Norwegian Fjord Areas: Examples, Spatial Distribution and Temporal Pattern, in: Evans, S.G., Scarascia Mugnozza, G., Strom, A. and Hermanns, R.L. (Eds.), Landslides from Massive Rock Slope Failure; NATO Science Series, IV. Earth and Environmental Sciences, v. 49. Springer, Dodrecht, Netherlands, pp. 475-496.

Blikra, L.H., Böhme, M., Dehls, J., Hermanns, R.L., Oppikofer, T., Redfield, T., Rønning, J.S., Yugsi Molina, F., Domaas, U., Pfaffhuber, A., Henriksen, H., Hole, J., and Kristensen, L., 2013.

The unstable phyllitic rocks in Stampa - Flåm, western Norway: Compilation, scenarios, risk and recommendations. NVE report no. 35-2013, Norwegian Water Resources and Energy Directorate, Oslo, Norway.

Blikra, L.H., Majala, G., Anda, E., Berg, H., Eikenæs, O., Helgås, G., Oppikofer T., Hermanns, R., and Böhme, M., 2016. Fare-og risikoklassifisering av ustabile fjellparti. Faresoner, arealhandtering og tiltak. NVE report no. 77-2016, Norwegian Water Resources and Energy Directorate, Oslo, Norway.

Böhme, M., Hermanns, R.L., Oppikofer, T., Fisher, L., Bunkholt, H.S.S., Eiken, T., Pedrazzini, A., Derron, M.-H., Jaboyedoff, M., Blikra, L.H., and Nilsen, B., 2013. Analysing complex rock slope deformation at Stampa, western Norway, by integrating geomorphology, kinematics and numerical modelling. Engineering Geology, v. 154, 116-130.

Braathen, A., Blikra, L.H., Berg, S.S., and Karlsen, F., 2004. Rock-slope failure in Norway; type, geometry, deformation mechanisms and stability. Norwegian Journal of Geology, v. 84, no. 1, 67-88.

Bryhni, I., 1977. Berggrunnskart 1416-4, Aurland – M. 1:50.000. Preliminært Berggrunnskart. Norges Geologiske Undersøkelse.

Bründl, M., Romang, H. E., Bischof, N., and Rheinberger, C. M., 2009. The risk concept and its application in natural hazard risk management in Switzerland, Nat. Hazards Earth Syst. Sci., 9, 801–813, https://doi.org/10.5194/nhess-9-801-2009.

Devoli, G., Eikenæs, O., Taurisano, A., Hermanns, R.L., Fischer, L., Oppikofer, T., and Bunkholt, H.S.S., 2011. Plan for skredfarekartlegging – Delrapport steinsprang, steinskred og fjellskred. NVE rapport 15/2011, Norges vassdrags- og energidirektorat, Oslo, Norge.

Domaas, U., Rosenvold, B.S., Blikra, L.H., Johansen, H., Grimstad, E., Sørlie, J.E., Gunleiksrud, O., Engen, A., and Lægreid, O., 2002: Studie av fjellskred og dalsidestabilitet i fyllittområder (Report to the Norwegian Research Council). Norwegian Geotechnical Institute Report 20001132-32.

Glimsdal, S., 2022. Flodbølger etter skred fra Stiksmoen, Aurland kommune. Beregning av faresoner. Norwegian Geotechnical Institute, Report 20210580-01-R.

Grimstad, E., 1987. RV. 601 Aurland-Fretheim. Geologisk vurdering av sammehengende tunnel forbi fretheimshaugane I Flåm. Norwegian Geotechnical Institute, Report 87618.

Grimstad, E., 1978. Rv. 601 Fretheim-Aurland tunnel eller skjæring øst for Flåm. Statens Vegvesen, Veglaboratoriet.

Hermanns, R.L., Bunkholt, H., Böhme, M., Fischer, L., Oppikofer, T., Rønning, J.S., and Eiken, T., 2011a. Foreløping fare- og risikovurdering av ustabile fjellparti ved Joasete-Furekamben-Ramnanosi, Aurland kommune. NGU report no. 2011.025, Geological Survey of Norway, Trondheim, Norway.

Hermanns, R.L., Fischer, L., Oppikofer, T., Böhme, M., Dehls, J.F., Henriksen, H., Booth, A., Eilertsen, R., Longva, O., and Eiken, T., 2011b. Mapping of unstable and potentially unstable slopes in Sogn og Fjordane (work report 2008-2010). NGU report no. 2011.55, Geological Survey of Norway, Trondheim, Norway.

Hermanns, R.L., Oppikofer, T., Anda, E., Blikra, L.-H., Böhme, M., Bunkholt, H., Crosta, G., Dahle, H., Devoli, G., Fischer, L., Jaboyedoff, M., Löew, S., Sætre, S., and Yugsi Molina, F., 2012. Recommended hazard and risk classification system for large unstable rock slopes in Norway. NGU report no. 2012.029, Geological Survey of Norway, Trondheim, Norway.

Hungr, O., and Evans, S.G., 1996. Rock avalanche runout prediction using a dynamic model. In: Senneset, K. (Ed.). Proceedings of the 7th International Symposium on Landslides, Trondheim, Norway, v. 1, 233-238.

Hungr, O., and McDougall, S., 2009. Two numerical models for landslide dynamic analysis. Computers & Geosciences, v. 35, 978-992.

NGU, 2020. Nasjonal database for ustabile fjellparti. http://geo.ngu.no/kart/ustabilefjellparti/ Geological Survey of Norway, Trondheim, Norway.

Massonnet, D., and Feigl, K.L., 1998. Radar interferometry and its application to changes in the earth's surface: Reviews of Geophysics, v. 36, p. 441–500.

Mazzanti, P., and Bozzano, F., 2011. Revisiting the February 6th 1783 Scilla (Calabria, Italy) landslide and tsunami by numerical simulation. Marine Geophysics Research, v. 32, 273-286.

Mazzanti, P., Bozzano, F., Avolio, M.V., Lupiano, V., and Di Gregorio, S., 2010. 3D Numerical Modelling of Submerged and Coastal Landslide Propagation. Advances in Natural and Technological Hazards Research, v. 28, 127-139.

McDougall, S., and Hungr, H., 2004. A model for the analysis of rapid landslide motion across three-dimensional terrain. Canadian Geotechnical Journal, v. 41, 1084-1097.

Nicolaisen, K.W., 2020. En Flåm av turister. En studie av stedets betydning for lokalbefolkningen i en turistbygd. Institute of Geography, University of Bergen. Master Thesis. 131 p.

Nicolet, P., 2017. Quantitative risk analysis for natural hazards at local and regional scales. PhD Thesis, University of Lausanne. https://serval.unil.ch/notice/serval:BIB_72FA1F0DF666

Oppikofer, T., Hermanns, R.L., Roberts, N., and Böhme, M., 2016a. SPLASH: semi-empirical prediction of landslide-generated displacement wave run-up heights. In Lintern et al., eds. Subaqueous Mass Movements and their consequences: Assessing Geohazards, Environmental Implications and Economic Significance of Subaqueous Landslides. Geological Society of London, Special Publications. https://doi.org/10.1144/SP477.1

Oppikofer, T., Böhme, M., Nicolet, P., Penna, I., and Hermanns, R., 2016b. Metodikk for konsekvensanalyse av fjellskred. NGU report no. 2016.047, Geological Survey of Norway, Trondheim, Norway.

Oppikofer, T., Hermanns, R.L., Jakobsen, V.U., Böhme, M., Nicolet, P., and Penna, I., 2021. Semi-empirical prediction of dam height and stability of dams formed by rock slope failures in Norway. Natural Hazards and Earth Science System, v. 20., p. 3179-3196.

Penna, I., Böhme, M., and Hermanns, R., 2017. Dynamic modelling with DAN3D of Stampa Scenario 3A. NGU report no. 2017.018, Geological Survey of Norway, Trondheim, Norway.

Scheidegger, A.E., 1973. On the prediction of the reach and velocity of catastrophic landslides. Rock Mechanics, v. 5, p. 231-236.

Sosio, R., Crosta, G.B., and Hungr, O., 2008. Complete dynamic modeling calibration for the Thurwieser rock avalanche (Italian Central Alps). Engineering Geology, v. 100, 11-26.

Tassis, G., and Larsen, B.E., 2021. ERT and GPR survey at the Stiksmoen unstable rock slope, Aurland municipality, Vestland county. NGU report no. 2021.025, Geological Survey of Norway, Trondheim, Norway.

Øydvin, E., Devoli, G., Bargel, T.H., Wiig, T., Taurisano, A., Berg, H., Eikenæs, O., Lyche, E., Fergus, T., Kvakland, M.R., Wasrud, J., Helle, T.E., Orvedal, K., Peereboom, I.O., Anderson, Ø., Hermanns, R.L., Høst, J., Hansen, L., Bunkholt, H.S., Eilertsen, R., Fischer, L., L'Heuraux, J.-S., Oppikofer, T., Rubensdotter, L., Sletten, K., Solberg, I.-L., and Stalsberg, K., 2011. Plan for skredfarekartlegging. Status og prioriteringer innen oversiktskartlegging og detaljert skredfarekartlegging i NVEs regi. NVE rapport 14/2011, Norges vassdrags- og energidirektorat, Oslo, Norge.

Appendix 1

Ap.Table 1. Type of buildings included in the hazard zones for displacement waves modelled by Glimsdal (2022).

Hazard zone		SOSI code	Bygningstype
1/1000	1/5000		
1	4	111	Enebolig
	1	159	Annen bygning for bofellesskap
5	6	161	Hytter, sommerhus, fritidsbygg
1	1	171	Seterhus, sel, rorbu o.l.
4	7	181	Garasje ,uthus, anneks knyttet til bolig
	1	182	Garasje, uth., anneks knyttet til fritidbolig
18	25	183	Naust, båthus, sjøbu
1	2	199	Annen boligb. (eks. sekundærbolig reindrift)
1	1	212	Verkstedbygning
1	1	214	Bygning for renseanlegg
1	1	231	Lagerhall
1	2	239	Annen lagerbygning
1	2	241	Hus for dyr/landbrukslager/silo
2	2	245	Naust/redskapshus for fiske
1	1	249	Annen landbruksbygning
3	3	312	Bankbygning, posthus
	1	319	Annen kontorbygning
3	3	322	Butikk/forretningsbygning
1	1	329	Annen forretningsbygning
1	1	412	Jernbane- og T-banestasjon
2	2	419	Annen ekspedisjons- og terminalbygning
2	2	439	Annen garasje-/hangarbygning
1	4	511	Hotellbygning
1	1	519	Annen hotellbygning
1	1	521	Hospits, pensjonat
1	1	523	Appartement
1	1	524	Camping-/utleiehytte
3	3	531	Restaurantbygning, kafébygning
1	1	539	Annen restaurantbygning
1	1	641	Museum, kunstgalleri
1	1	840	Offentlig toalett

Note: Bygningstyper (based on NS 3457)

Ap.Figure 1. Hazard analysis and ranking of parameters considered for the classification.

Fareklasser	Sannsynlighet	Kum. sannsyn.
Meget lav	0.0 %	0.0 %
Lav	0.0 %	0.0 %
Medium	4.1 %	4.1 %
Høy	80.5 %	84.6 %
Meget høy	15.4 %	100.0 %

Farepoeng	
Minimum	6.50
Maksimum	11.00
Modus	8.50
Gjennomsnitt	8.70
5% persentil	7.08
95% persentil	9.97

Tilpasset normalfordeling	
Gjennomsnitt	8.58
Standardavvil	0.90
$\mu - 2\sigma$	6.78
$\mu + 2\sigma$	10.38
Korr.-koeff.	0.9999
K-S-test	2.0 %

Kriteria (poeng)	Relativ sannsynlighet					
1. Bakskrent (0 / 0.5 / 1)	0	0	1			
2. Potensielle glidestrukturer (0 / 0.5 / 1)	0	1	2			
3. Flanker (0 / 0.25 / 0.5 / 0.75 / 1)	0	0	0	2	1	
4. Kinematisk analyse (0 / 0.5 / 0.75 / 0.75 / 1)	0	0	0	2	1	
5. Morfologisk tegn på bruddflaten (0 / 0.5 / 1)	0	1	2			
6. Bevegelseshastighet (0 / 1 / 2 / 3 / 4 / 5)	0	0	1	1	0	0
7. Akselerasjon (0 / 1)	4	1				
8. Økning av steinsprangsaktivitet (0 / 1)	1	2				
9. Tidligere hendelser (0 / 0.5 / 1)	0	0	1			

Ap.Figure 2. Hazard ranking, scores and considerations.

Farevurdering av ustabile fjellpartier i Norge

Lokalitetens navn:	Stiksmoen	Scenario:		Utført av:	I. Penna	Dato:		1/17/2022	

Fareklasser	Sannsynlighet	Kumul. sannsyn.		Farepoeng			Tilpasset normalfordeling	
Meget lav	0.0 %	0.0 %		**Minimum**	6.5		**Gjennomsnitt μ**	8.6
Lav	0.0 %	0.0 %		**Maksimum**	11.0		**Standardavvik σ**	0.9
Middels	4.1 %	4.1 %		**Modus**	8.5		**μ - 2σ**	6.8
Høy	80.5 %	84.6 %		**Gjennomsnitt**	8.7		**μ + 2σ**	10.4
Meget høy	15.4 %	100.0 %		**5% persentil**	7.1		**Korrelasjonskoeff.**	0.9999
				95% persentil	10.0		**K-S-test**	2.0 %

1. Bakskrent								Poeng	Norm. sannsyn.
Ikke utviklet								0	0.0 %
Delvis åpen over bredden av det ustabile fjellpartiet (få cm til m)								0.5	0.0 %
Fullstendig åpen over bredden av det ustabile fjellpartiet (få cm til m)								1	100.0 %
Kommentar:	Well developed backscarp. Max. opening of ca. 9 meters, unknown depth (depression filled with blocks from the unstable rock mass, glaciomarine sediments removed from Sletta, and trash). Developed in the central and northern part along foliation.								

2. Potensielle glidestrukturer								Poeng	Norm. sannsyn.
Ingen gjennomsettende strukturer er utgående i fjellsiden								0	0.0 %
Gjennomsettende strukturer faller gjennomsnittlig <20 grader eller er brattere enn fjellsiden								0.5	33.3 %
Gjennomsettende strukturer faller gjennomsnittlig >20 grader og er utgående i fjellsiden								1	66.7 %
Kommentar:	Developed mainly along foliation, breaking through along axis of small folds. Graphite layers at the toe of the unstable rock mass. Dip: 30-40 degrees.								

3. Flanker								Poeng	Norm. sannsyn.
Ikke utviklet								0	0.0 %
Delvis utviklet på 1 side								0.25	0.0 %
Fullstendig utviklet eller åpen skråning på 1 side eller delvis utviklet på 2 sider								0.5	0.0 %
Fullstendig utviklet eller åpen skråning på 1 side og delvis utviklet på 1 sider								0.75	66.7 %
Fullstendig utviklet eller åpen skråning på 2 sider								1	33.3 %
Kommentar:	The northern flank is free. The southern flank is less developed and in parts covered by scree material.								

4. Kinematisk analyse								Poeng	Norm. sannsyn.
Kinematisk mulighetstest tillater ikke planutglidning, kileutglidning eller utvelting								0	0.0 %
Brudd er delvis kinematisk mulig (bevegelsesretning er > ±30° i forhold til skråningsorientering)								0.5	0.0 %
Brudd er kinematisk mulig (bevegelsesretning er <= ±30° i forhold til skråningsorientering)								0.75	0.0 %
Brudd er delvis kinematisk mulig på utholdende svakhetsplan (bevegelsesretning er > ±30° i forhold til skråningsorientering)								0.75	66.7 %
Brudd er kinematisk mulig på utholdende svakhetsplan (bevegelsesretning er <= ±30° i forhold til til skråningsorientering)								1	33.3 %
Kommentar:	Complex planar sliding along foliation that dips 30-40 degrees towards the fjord. Structural measurements indicate planar sliding as most probable mechanism, but wedge failure is possible. The NGI report proposes a kind of planar sliding along foliation that dips 30-40 degrees towards the fjord.								

5. Morfologisk tegn på bruddflaten								Poeng	Norm. sannsyn.
Ingen indikasjon i morfologien								0	0.0 %
Morfologi av skråningen tyder på utviklingen av en bruddflate (utbulning, konkavitet-konveksitet, vannkilder)								0.5	33.3 %
Sammenhengende bruddflate er antydet i skråningens morfologi og kan kartlegges								1	66.7 %
Kommentar:	The location of the lower limit is relatively well constrained. Graphite horizons observed, slope break and geophysical survey indicating it.								

6. Bevegelseshastighet								Poeng	Norm. sannsyn.
Ingen signifikant bevegelse								0	0.0 %
>0 - 0.5 cm/år								1	0.0 %
0.5 - 1 cm/år								2	50.0 %
1 - 4 cm/år								3	50.0 %
4 - 10 cm/år								4	0.0 %
> 10 cm/år								5	0.0 %
Kommentar:	Between 0.9 and 1.5 cm/y measured with extensometers. dGNSS, InSAR and GBInSAR of around 2.5 cm/y. Category 1-4 cm/y in the NGU classification system but with some weight to the class 0.5-1 cm/y.								

7. Akselerasjon (hvis bevegelsen er >0.5 cm/år og <10 cm/år)								Poeng	Norm. sannsyn.
Ingen akselerasjon eller endring i bevegelseshastigheten								0	80.0 %
Økning i bevegelseshastigheten								1	20.0 %
Kommentar:	The available information cannot be used to confirm or rule out acceleration. Current measurements seem to be higher than those measured by NGI with extensometers. However, measurement methods were different and took place on different parts of the unstable rock mass. NGI placed most of the bolts for measuring with extensometers on the upper sector presenting most of the fragmented blocks. Therefore they have measured compartments and may not cover the entire displacement.								

8. Økning av steinsprangsaktivitet								Poeng	Norm. sannsyn.
Ingen økning av steinsprangsaktivitet								0	33.3 %
Økt steinsprangsaktivitet								1	66.7 %
Kommentar:	More rockfall activity than in the surroundings. Retention wall along the road.								

9. Tidligere hendelser								Poeng	Norm. sannsyn.
Ingen postglasiale hendelser av liknende størrelse								0	0.0 %
En eller flere hendelser av lignende størrelse eldre enn 5000 år								0.5	0.0 %
En eller flere hendelser av lignende størrelse yngre enn 5000 år								1	100.0 %
Kommentar:	The occurrence of past events is well known in the eastern slope of Aurlandfjord between Stampa and Ramnanosi. A small collapse, immediately north of the instability, is observed in bathymetric data. It is well preserved and only partially buried with sediments.								

Ap.Figure 3. Risk classification – combination of hazard zones.

	Consequences			Probability		Risk		
	min	avg	max	original	partial	min	avg	max
Direct impact	3.5	5	8	0.0034807	0.00124035	0.004341	0.006202	0.009923
1/1000	70.455	565.1621	1620.52	0.00224035	0.00164035	0.115571	0.927064	2.65822
1/5000	96.81	613.8471	1839.69	0.0006	0.0006	0.058086	0.368308	1.103814
					0.0034807	0.177998	1.301574	3.771957
Corresponding number of deaths for the initial probability -->						51.13859	373.9402	1083.678

GEOLOGICAL
SURVEY OF
NORWAY
· NGU ·